Bioorganic Chemistry 57 (2014) 13–29

Contents lists available at ScienceDirect

Bioorganic Chemistry

journal homepage: www.elsevier.com/locate/bioorg

Novel trisubstituted acridines as human telomeric quadruplex binding ligands

Jan Ungvarsky [b], Jana Plsikova [a,e], Ladislav Janovec [b], Jan Koval [c], Jaromir Mikes [c], Lucia Mikesová [c], Denisa Harvanova [e], Peter Fedorocko [c], Pavol Kristian [b], Jana Kasparkova [d], Viktor Brabec [d], Maria Vojtickova [b], Danica Sabolova [a], Zuzana Stramova [a], Jan Rosocha [e], Jan Imrich [b], Maria Kozurkova [a,*]

[a] Department of Biochemistry, Moyzesova 11, 04001 Kosice, Slovak Republic
[b] Department of Organic Chemistry, Moyzesova 11, 04001 Kosice, Slovak Republic
[c] Department of Cellular Biology, Moyzesova 11, 04001 Kosice, Slovak Republic
[d] Institute of Biophysics, Department of Molecular Biophysics and Pharmacology, Academy of Sciences of the Czech Republic, Brno, Czech Republic
[e] Associated Tissue Bank of Faculty of Medicine, L. Pasteur University Hospital, Trieda SNP 1, 04166 Kosice, Slovak Republic

ARTICLE INFO

Article history:
Received 8 April 2014
Available online 10 August 2014

Keywords:
Braco 19 derivatives
Trisubstituted acridines
DNA binding
G-quadruplex structures
Cell proliferation

ABSTRACT

A novel series of trisubstituted acridines were synthesized with the aim of mimicking the effects of BRACO19. These compounds were synthesized by modifying the molecular structure of BRACO19 at positions 3 and 6 with heteroacyclic moieties. All of the derivatives presented in the study exhibited stabilizing effects on the human telomeric DNA quadruplex. UV–vis spectroscopy, circular dichroism, linear dichroism and viscosimetry were used in order to study the nature of the DNA binding in more detail. The results show that all of the novel derivatives were able to fold the single-stranded DNA sequences into antiparallel G-quadruplex structures, with derivative **15** exhibiting the highest stabilizing capability. Cell cycle analysis revealed that a primary trend of the "braco"-like derivatives was to arrest the cells in the S- and G_2M-phases of the cell cycle within the first 72 h, with derivative **13** and BRACO19 proving particularly effective in suppressing cell proliferation. All studies derivatives were less toxic to human fibroblast cell line in comparison with HT 29 cancer cell line.

1. Introduction

The non-canonical nucleic acid structures known as G-quadruplexes show an extremely high level of stability which is derived in part from the stacking together of G-quartets through π–π interactions to form stable quadruplex motifs [1,2]. G-rich telomeric DNA folded into quadruplex has been the focus of much recent interest as a potential anti-cancer target due to its interaction with the ribonucleoprotein telomerase, an enzyme which maintains chromosomal integrity and which is up-regulated in approximately more than 85% of various human cancer cells [3]. As the inhibition of telomerase induces cell senescence, this process has become a target for potential anticancer therapeutic intervention [4,5] both *in vitro* and *in vivo* [6,7]. The telomerase substrate must be single-stranded in order to be recognized by the telomerase RNA template prior to the catalytic step in the telomere elongation cycle. Indirect inhibition of telomerase can be achieved by the telomeric DNA substrate folding into four stranded guanine quadruplex structures, using small molecule quadruplex-binding compounds [8]. The resultant folded substrate is unable to hybridize with the telomeric RNA template and the ability of telomerase to catalyze the synthesis of further telomeric DNA repeats is inhibited. The majority of quadruplex-binding compounds contain an extended planar aromatic chromophore [9]. It has been reported that quadruplex-binding trisubstituted acridines have exhibited rapid antitumor effects [10–12] involving several parallel mechanisms, including telomere uncapping [13–15], direct or indirect telomerase inhibition with the characteristic induction of senescence and of apoptosis. Recent research has also shown that G-quadruplexes selectively target both telomerase and telomere in cancer cells [16–18].

BRACO19 has shown some promising results in studies involving tumor cell cultures and mouse xenografts. It has been reported that treatment with BRACO19 resulted in both telomerase inhibition and also in general telomere dysfunction that led to atypical mitosis and consequently to apoptosis [1].

In this paper, we present a novel series of acridine based compounds as structural analogs of BRACO19. Based on findings from

* Corresponding author.
E-mail address: maria.kozurkova@upjs.sk (M. Kozurkova).

http://dx.doi.org/10.1016/j.bioorg.2014.07.010
0045-2068/

our previous results [19–23], the side chains at positions 3 and 6 of the initial braco structure were modified with thiourea, urea and guanidine. Molecular dynamics simulations were also used prior to the empirical examination of the interaction forces of the synthesized structures.

Although the synthesis of 3,6,9-trisubstituted acridines using 2,2′,4,4′-tetranitrobenzophenone has been described previously [24], we also aimed to elaborate the synthetic pathway including Ullmann-Jourdan coupling which would allow us to utilize a broad structural diversity of commercially available reactants in our future research.

2. Materials and methods

2.1. Chemicals and instruments

All chemicals and reagents were purchased of reagent grade and used without further purification. Ethidium bromide, dimethyl sulfoxide (DMSO), Triton X 100, Tris(hydroxymethyl) aminomethane (Tris) and calf thymus DNA were obtained from Sigma–Aldrich Chemie (Germany). EDTA, RNase A and proteinase K were purchased from Serva (Germany), and all other chemicals were purchased from Lachema (Czech Republic). DNA oligomers were obtained from Metabion. Braco19 was synthetized according to previously described procedure [24].

^{1}H (400 MHz, 600 MHz) and ^{13}C (100 MHz, 150 MHz) NMR spectra were measured on a Varian Mercury Plus or a Varian VNMRS NMR spectrometers at room temperature in CD_3OD or DMSO-d_6 using TMS as an internal standard (0 ppm for both nuclei). Melting points were determined with a Koffler hot-stage apparatus and are uncorrected. Elemental analyses were performed on a Perkin-Elmer analyzer CHN 2400. Reactions were monitored by thin-layer chromatography (TLC) using Silufol plates with detection at 254 nm. Preparative column chromatography was conducted using Kiesegel Merck 60 column, type 9385 (grain size 250 nm) or aluminum oxide Merck 90 neutral (grain size 200 nm).

2.2. Synthesis of trisubstituted acridine derivatives

2.2.1. Synthesis of 3-nitroacetanilide (**2**)

3-Nitroaniline (**1**) (1 g, 7.24 mmol) was heated to 100 °C in 5 mL of acetanhydride. The reaction was monitored with TLC, using toluene–acetone mixture (5:2 v/v) as eluent. After the reaction had finished, the reaction mixture was poured into water and neutralized by ammonium hydroxide. The precipitate was filtered off and used without purification in the next reaction.

Yield: 70%, white solid, mp: 156–158 °C. Anal. Calcd for $C_8H_8N_2O_3$ (180.16): 53.33% C, 4.48% H, 15.55% N. Found: 53.45% C, 4.25% H, 15.63% N. ^{1}H NMR (400 MHz, DMSO-d_6): 10.43 (s, 1H, NH), 8.63 (t, 1H, H-2, J = 1.60), 7.90 (d, 1H, H-6, J = 2.00), 7.88 (d, 1H, H-4, J = 2.00), 7.59 (t, 1H, H-5, J = 8.00), 2.11 (s, 3H, CH_3—CO). ^{13}C NMR (100 MHz, DMSO-d_6): 169.01 (C═O), 147.89 (C1), 140.33 (C3), 130.01 (C5), 124.80 (C6), 117.44 (C4), 112.93 (C2), 23.08 (CH_3—CO).

2.2.2. Synthesis of 3-aminoacetanilide (**3**)

Acetanilide **2** (1 g, 5.66 mmol) was dissolved in 100 mL of methanol and a catalytic amount of 10% palladium on activated charcoal (ca. 0.015 g) was added. The reaction mixture was cooled by an ice bath and natrium borohydride (1 g, 26.43 mmol) was added portionly. The resulting mixture was then stirred vigorously for 1 h. The end of the reaction was monitored with TLC, using toluene–acetone mixture (5:2 v/v) as eluent. The product was chromatographed over silica gel eluated by toluene–acetone mixture (5:2 v/v).

Yield: 75%, white solid, mp: 86–88 °C. Anal. Calcd for $C_8H_{10}N_2O$ (150.18): 63.98% C, 6.71% H, 18.65% N. Found: 63.76% C, 6.50% H, 18.53% N. ^{1}H NMR (400 MHz, DMSO-d_6): 9.58 (s, 1H, NH), 6.92 (t, 1H, H-2, J = 2.00), 6.88 (t, 1H, H-4, J = 8.00), 6.64 (dd, 1H, H-6, J_1 = 0.80, J_2 = 8.00), 6.23 (dd, 1H, H-5, J_1 = 1.60, J_2 = 8.00), 5.00 (bs, 2H, NH_2), 1.99 (s, 3H, CH_3—CO). ^{13}C NMR (100 MHz, DMSO-d_6): 167.85 (C═O), 148.85 (C1), 139.85 (C3), 128.75 (C4), 109.04 (C5), 106.93 (C6), 104.67 (C2), 23.98 (CH_3—CO).

2.2.3. Synthesis of 4-(acetylamino)-2-chlorotoluene (**5**)

A solution of acetyl chloride (0.83 g, 10.59 mmol) in 10 mL of dry methylene chloride was added in drops over 20 min into the solution of 4-amino-2-chlorotoluene (**4**) (1 g, 7.06 mmol) and triethylamine (1.43 g, 14.12 mmol) in 10 mL of dry methylene chloride. Once the full amount of acetyl chloride had been added, the reaction mixture was stirred until the reaction was completed according to TLC, using toluene–acetone mixture (5:2 v/v) as eluent. In order to eliminate an excess of acetyl chloride, 5 mL of methanol was then added to the reaction mixture. After 15 min, the solvent was evaporated off at reduced pressure, and the crude product was dissolved in 10 mL of methanol and slowly poured into distilled water. The thus-obtained precipitate **5** was filtered off and dried overnight.

Yield: 95%, white solid, mp: 105–106 °C. Anal. Calcd for $C_9H_{10}ClNO$ (183.64): 58.86% C, 5.49% H, 7.63% N. Found: 58.98% C, 5.35% H, 7.77% N. ^{1}H NMR (400 MHz, DMSO-d_6): 10.01 (s, 1H, NH), 7.78 (d, 1H, H-2, J = 2.00), 7.33 (dd, 1H, H-6, J_1 = 2.00, J_2 = 8.40), 7.23 (d, 1H, H-5, J = 8.4), 2.25 (s, 3H, CH_3), 2.03 (s, 3H, CH_3—CO). ^{13}C NMR (100 MHz, DMSO-d_6): 168.32 (C═O), 138.36 (C1), 132.83 (C3), 130.99 (C5), 129.41 (C4), 118.81 (C2), 117.45 (C6), 23.87 (CH_3—CO), 18.80 (CH_3).

2.2.4. Synthesis of 4-(acetylamino)-2-chlorobenzoic acid (**6**)

Acetamide **5** (1 g, 5.45 mmol) was added to a solution of potassium permanganate (2.58 g, 16.34 mmol) in 100 mL of distilled water. The reaction mixture was stirred vigorously at reflux temperature for 2 h. The reaction was monitored with TLC, using toluene–acetone mixture (3:2 v/v) as eluent. After the reaction was completed, the resultant mixture was filtered in order to remove manganese dioxide and the filtrate was acidified with diluted hydrochloric acid (1:3 v/v) thereby producing the acid **6** from its potassium salt. The precipitated product **6** was then suction-filtered though a Büchner funnel and dried overnight.

Yield: 65%, white solid, mp: 208–210 °C. Anal. Calcd for $C_9H_8ClNO_3$ (213.62): 50.60% C, 3.77% H, 6.56% N. Found: 50.70% C, 3.58% H, 6.62% N. ^{1}H NMR (400 MHz, DMSO-d_6): 10.35 (s, 1H, NH), 7.88 (d, 1H, H-3, J = 2.00), 7.83 (d, 1H, H-6, J = 8.40), 7.53 (dd, 1H, H-5, J_1 = 2.00, J_2 = 8.40), 2.09 (s, 3H, CH_3). ^{13}C NMR (100 MHz, DMSO-d_6): 169.04 (C═O), 165.84 (COOH), 142.78 (C4), 132.93 (C2), 132.27 (C3), 124.29 (C1), 119.87 (C6), 116.68 (C5), 24.06 (CH_3).

2.2.5. Synthesis of 4-(acetylamino)-2-(3-(acetylamino)phenylamino)benzoic acid (**7**)

Dry potassium carbonate (0.32 g, 2.34 mmol), activated copper (0.029 g, 0.46 mmol) and copper(I) oxide (0.06 g, 0.43 mmol) were added to a mixture of benzoic acid **6** (1 g, 4.68 mmol) and 3-aminoacetanilide (**3**) (0.77 g, 5.15 mmol) in 8 mL of ethoxyethanol. After 4 h of vigorous stirring at reflux temperature, the reaction mixture was poured into 30 mL of distilled water and the resultant mixture was filtered. The filtrate was than acidified with hydrochloric acid (1:3 v/v) and the precipitated crude product was suction-filtered though a Büchner funnel and dried overnight.

Yield: 50%, white solid, mp: 254–255 °C. Anal. Calcd for $C_{17}H_{17}N_3O_4$ (327.34): 62.38% C, 5.23% H, 12.84% N. Found: 62.50% C, 5.15% H, 12.74% N. ^{1}H NMR (400 MHz, DMSO-d_6):

12.75 (bs, 1H, OH), 10.07 (s, 1H, NH″), 9.96 (s, 1H, NH′), 9.69 (s, 1H, NH-Acr), 7.83 (d, 1H, H-6, J = 8.80), 7.56 (d, 1H, H-3, J = 1.60), 7.48 (s, 1H, H-2′), 7.29 (dd, 1H, H-4′, J_1 = 3.20, J_2 = 8.00), 7.27 (t, 1H, H-5′ J = 8.00), 7.07 (dd, 1H, H-5, J_1 = 2.00, J_2 = 8.80), 6.96 (d, 1H, H-6′, J = 7.60), 2.05 (s, 3H, CH_3), 2.02 (s, 3H, CH_3′). ^{13}C NMR (100 MHz, DMSO-d_6): 169.55 (COOH), 168.73 (CO′), 168.25 (CO), 147.78 (C2), 144.37 (C4), 140.63 (C1′), 140.38 (C3′), 132.70 (C6), 129.48 (C5′), 115.76 (C6′), 113.72 (C4′), 112.01 (C2′), 108.37 (C5), 107.09 (C1), 102.60 (C3), 24.09 (CH_3′), 23.98 (CH_3).

2.2.6. Synthesis of 3,6-diamino-9(10H)-acridone (**9a**) and 1,6-diamino-9(10H)-acridone (**9b**)

Benzoic acid (**7**) (20 g, 61.1 mmol) was added to 80 mL of 96% sulfuric acid in a 250 mL round flask, in small amounts over a 15 min period. The resultant mixture was then heated to 100 °C in an oil bath. After 3 h of intensive stirring, the mixture was removed from the oil bath and cooled to room temperature. The reaction mixture was then poured onto 300 g of ice in a 1 L beaker. The crude mixture was alkalized with concentrated sodium hydroxide to pH 12–13 and then suction-filtered though a Büchner funnel and dried overnight. The resultant mixture of acridones was used in the next reaction step without further purification.

2.2.7. Synthesis of 3,6-bis(butanoylamino)-9(10)-acridone (**10**)

A mixture of diaminoacridones **9a** and **9b** (10 g, 4.44 mmol) was added to 70 mL of butyric anhydride (62.5 mmol) in a 250 mL round flask. The reaction mixture was heated to 100 °C in an oil bath and stirred vigorously for 2 h. Once the resultant mixture had cooled to room temperature, 30 mL of acetone was added. The mixture was poured into 200 mL of brine with an additive of 15 mL of saponate. A concentrated solution of sodium hydroxide was added to the mixture in 25 mL portions over 15 min, until an alkaline pH had been achieved. The precipitated product was suction-filtered though a Büchner funnel, washed with distilled water and dried overnight. The crude mixture was refluxed in 300 mL of acetone in order to dissolve 1,6-isomer and separate it from 3,6-isomer **10**. After 3 h, the mixture containing the little soluble 3,6-isomer **10** was suction-filtered though a Büchner funnel.

Yield: 55%, gray solid, mp > 300 °C. Anal. Calcd for $C_{21}H_{23}N_3O_3$ (365.43): 69.20% C, 6.34% H, 11.50% N. Found: 69.08% C, 6.25% H, 11.63% N. ^{1}H NMR (400 MHz, DMSO-d_6): 11.63 (s, 1H, NH), 10.25 (s, 2H, 2×NH—CO), 8.15 (s, 2H, H-4,5), 8.09 (d, 2H, H-1,8, J = 8.40), 7.20 (d, 2H, H-2,7, J = 8.40), 2.37 (t, 4H, 2×CH_2—CO, J = 6.80), 1.65 (m, 4H, 2×CH_2), 0.95 (t, 6H, 2×CH_3, J = 7.20). ^{13}C NMR (100 MHz, DMSO-d_6): 174.89 (CO), 171.84 (2×NH—CO), 143.14 (C4a, C10a), 142.02 (C3, C6), 126.70 (C1, C8), 116.27 (C8a, C9a), 113.14 (C2, C7), 104.55 (C4, C5), 38.42 (2×CH_2—CO), 18.45 (2×CH_2), 13.55 (2×CH_3).

2.2.8. Synthesis of 3,6-bis(butanoylamino)-9-chloroacridine (**11**)

Acridone **10** (5 g, 13.7 mmol) as a fine powder was slowly added to 20 mL of $POCl_3$ (21.5 mmol) over 15 min. The resultant mixture was then heated to 70 °C in an oil bath and stirred vigorously. After 90 min, the resultant mixture was cooled to room temperature and slowly poured into 100 g of ice in 100 mL of distilled water, a process which resulted in the heating of the water. A concentrated solution of sodium hydroxide was added to the resultant mixture in 25 mL portions in 15 min intervals until an alkaline pH had been achieved. The precipitated product was suction-filtered though a Büchner funnel, washed with distilled water and dried overnight. The resultant crude product was crystallized from ethyl acetate.

Yield: 45%, light red solid, mp: 153–155 °C. Anal. Calcd for $C_{21}H_{22}ClN_3O_2$ (383.87): 65.71% C, 5.78% H, 10.95% N. Found: 65.53% C, 5.82% H, 10.87% N. ^{1}H NMR (400 MHz, DMSO-d_6): 10.45 (s, 2H, 2×NH—CO), 8.58 (d, 2H, H-4,5, J = 2.00), 8.27 (d, 2H, H-1,8, J = 9.60), 7.76 (dd, 2H, H-2,7, J_1 = 2.00, J_2 = 9.60), 2.43 (t, 4H, 2×CH_2—CO, J = 7.60), 1.70 (m, 4H, 2×CH_2), 0.98 (t, 6H, 2×CH_3, J = 7.60). ^{13}C NMR (100 MHz, DMSO-d_6): 172.08 (2×CO), 149.50 (C9), 141.24 (C4a, C10a), 139.13 (C3, C6), 124.81 (C1, C8), 121.69 (C2, C7), 119.34 (C8a, C9a), 113.58 (C4, C5), 38.46 (2×CH_2—CO), 18.34 (2×CH_2), 13.57 (2×CH_3).

2.2.9. Synthesis of 3,6-bis(butanoylamino)-9-[4′-(N,N-dimethylamino)phenylamino] acridine hydrochloride (**12**)

A mixture of 9-chloroacridine **11** (1 g, 2.60 mmol), *N,N*-dimethylbenzene-1,4-diamine (1.42 g, 10.41 mmol) and phenol (10 g, 106 mmol) was heated at 100 °C for 2 h. Brine (30 mL) was then poured into the reaction mixture and this resultant mixture was poured into 300 mL of water and alkalized with a concentrated solution of sodium hydroxide until a pH of 10 was achieved. The precipitated product was suction-filtered through a Büchner funnel, washed with distilled water and dried overnight. A product **12** was dissolved in methanol prior to the addition of an equimolar solution of HCl in acetone (acetone/36% HCl; 9:1 v/v), then it was stirred for 1 h, and filtered off as a hydrochloride salt.

Yield: 60%, red solid, mp > 300 °C. Anal. Calcd for $C_{29}H_{33}N_5O_2$. HCl (520.06): 66.97% C, 6.59% H, 13.47% N. Found: 67.05% C, 6.67% H, 13.32% N. ^{1}H NMR (600 MHz, CD_3OD): 8.61 (d, 2H, H-4,5, J = 1.80), 8.09 (d, 2H, H-1,8, J = 9.60), 7.74 (d, 2H, H-3′,5′, J = 8.40), 7.51 (d, 2H, H-2′,6′, J = 9.00), 7.38 (dd, 2H, H-2,7, J_1 = 1.80, J_2 = 9.00), 3.34 (s, 6H, 2×N-CH_3′), 2.47 (t, 4H, 2×CH_2—CO, J = 7.20), 1.76 (m, 4H, 2×CH_2), 1.03 (t, 6H, 2×CH_3, J = 7.80). ^{13}C NMR (150 MHz, CD_3OD): 175.44 (2×CO), 154.40 (C9), 146.60 (C4a, C10a), 144.16 (C1′), 143.77 (C3, C6), 141.75 (C4′), 127.86 (C1, C8), 125.74 (C2′, C6′), 123.07 (C3′, C5′), 119.18 (C2, C7), 112.55 (C8a, C9a), 106.21 (C4, C5), 46.97 (N-2×CH_3′), 40.06 (2×CH_2—CO), 19.93 (2×CH_2), 14.00 (2×CH_3).

2.2.10. Synthesis of 3,6-diamino-9-[4′-(N,N-dimethylamino)phenylamino]acridine (**13**)

A mixture of the derivative **12** (0.3 g, 0.62 mmol) and 98% H_2SO_4 (1.5 mL, 28 mmol) was stirred well at 100 °C for 15 min and then poured into 20 mL of distilled water. Active coal was stirred into the resultant mixture and later filtered off. The purified mixture was alkalized with the solution of sodium hydroxide until a product **13** was precipitated and subsequently filtered off.

Yield: 75%, red solid, mp: 235–237 °C. Anal. Calcd for $C_{21}H_{21}N_5$ (343.43): 73.44% C, 6.16% H, 20.39% N. Found: 73.31% C, 6.28% H, 20.50% N. ^{1}H NMR (600 MHz, CD_3OD): 7.70 (d, 2H, H-1,8, J = 9.00), 6.99 (d, 2H, H-2′,6′, J = 9.00), 6.77 (d, 2H, H-3′,5′, J = 9.60), 6.64 (d, 2H, H-4,5, J = 1.80), 6.58 (dd, 2H, H-2,7, J_1 = 2.40, J_2 = 9.60), 2.92 (s, 6H, 2×CH_3′). ^{13}C NMR (150 MHz, CD_3OD): 154.28 (C9), 152.13 (C4a, C10a), 149.85 (C4′), 147.28 (C3, C6), 135.01 (C1′), 127.95 (C1, C8), 124.94 (C2′, C6′), 115.49 (C2, C7), 115.10 (C3′, C5′), 108.79 (C8a, C9a), 99.30 (C4, C5), 41.36 (2×CH_3′).

2.2.11. Synthesis of 3,6-diisothiocyanato-9-[4′-(N,N-dimethylamino)phenylamino] acridine (**14**)

A mixture of the acridine **12** (0.3 g, 0.62 mmol) and 98% H_2SO_4 (1.5 mL, 28 mmol) was stirred well at 100 °C for 15 min and then poured into 20 mL of distilled water. The resultant mixture was neutralized with a concentrated solution of sodium hydrogen carbonate and used as a stock solution in the synthesis of a diisothiocyanate **14** without further purification. This stock solution of free amine **12** was added in drops to a well stirred mixture of thiophosgene (0.15 mL, 1.96 mmol) in 70 mL of chloroform at 0 °C. The resultant mixture was stirred vigorously at room temperature for 2 h. The organic layer was separated and the solvent was evaporated *in vacuo*. A crude product of the compound **14** was used without further purification in the synthesis of a corresponding thiourea **15**.

*2.2.12. Synthesis of 3,6-bis[3-(2-dimethylaminoethyl)thioureido]-9-[4′-(N,N-dimethylamino)phenylamino]acridine (**15**)*

The diisothiocyanate **14** (0.1 g, 0.23 mmol) was dissolved in 20 mL of chloroform and cooled to −20 °C. Triethylamine (0.4 mL, 2.86 mmol) and *N,N*-dimetylethylenediamine (0.07 mL, 0.64 mmol) were added to the mixture which was then placed in a freezer to react overnight. The end of the reaction was monitored with TLC (eluent MeOH/NH_4OH 50:4). Chloroform was evaporated *in vacuo* and a crude bisthiourea **15** was purified by column chromatography on silica gel eluted by a mixture of methanol–25% water solution of ammonia (50:4). After evaporation of the eluent *in vacuo*, the bisthiourea **15** was diluted with a small quantity of methanol and subsequently poured into a saturated solution of sodium hydrogencarbonate. The precipitate **15** was then filtered off.

Yield: 65%, brown solid, mp: 155–157 °C. Anal. Calcd for $C_{31}H_{41}N_9S_2$ (603.85): 61.66% C, 6.84% H, 20.88% N. Found: 61.55% C, 6.69% H, 20.80% N. ^{1}H NMR (600 MHz, CD_3OD): 7.97 (s, 2H, H-4,5), 7.78 (d, 2H, H-1,8, J = 7.20), 7.12 (s, 2H, 2H, H-2,7), 6.91 (d, 2H, H-2′,6′, J = 9.00), 6.73 (d, 2H, H-3′,5′, J = 8.40), 3.74 (s, 4H, 2×CH_2—NH), 2.90 (s, 6H, 2×CH_3′), 2.61 (t, 4H, 2×CH_2—N(CH_3)$_2$, J = 6.00), 2.30 (s, 12H, 4×CH_3). ^{13}C NMR (150 MHz, CD_3OD): 182.14 (2×C═S), 151.14 (C9), 149.58 (C4′), 147.39 (C4a, C10a), 143.74 (C3, C6), 136.26 (C1′), 127.00 (C1, C8), 124.26 (C2′, C6′), 119.66 (C2, C7), 115.17 (C3′, C5′), 114.40 (C4, C5), 113.58 (C8a, C9a), 58.54 (2×CH_2—N(CH_3)$_2$), 45.61 (4×CH_3), 43.10 (2×CH_2—NH), 41.45 (2×CH_3′).

*2.2.13. Synthesis of 3,6-bis[3-(2-dimethylaminoethyl)ureido]-9-[4′-(N,N-dimethylamino)phenylamino]acridine (**16**)*

Mesitylnitrile oxide (0.05 g, 0.33 mmol) was added to a suspension of the bisthiourea **15** (0.05 g, 0.08 mmol) in 7 mL of methanol and stirred well overnight at room temperature. A resultant bisurea **16** was filtered off and purified by column chromatography on silica gel eluted by a mixture of methanol–25% water solution of ammonia (50:4).

Yield: 30%, dark yellow solid, mp: 105–106 °C. Anal. Calcd for $C_{31}H_{41}N_9O_2$ (571.72): 65.13% C, 7.23% H, 22.05% N. Found: 65.25% C, 7.15% H, 21.99% N. ^{1}H NMR (600 MHz, CD_3OD): 7.64 (d, 2H, H-4,5, J = 1.20), 7.56 (d, 2H, H-1,8, J = 8.40), 7.09 (d, 2H, H-2′,6′, J = 9.00), 6.90 (d, 2H, H-2,7, J = 9.00), 6.76 (d, 2H, H-3′,5′, J = 8.40), 3.55 (t, 4H, 2×CH_2—NH, J = 6.60), 3.00 (t, 4H, 2×CH_2—N(CH_3)$_2$, J = 6.00), 2.98 (s, 6H, 2×CH_3′), 2.67 (s, 12H, 4×CH_3). ^{13}C NMR (150 MHz, CD_3OD): 157.07 (2×C═O), 153.90 (C9), 151.30 (C4′), 147.04 (C4a, C10a), 142.66 (C3, C6), 130.54 (C1′), 127.24 (C2′, C6′), 127.12 (C1, C8), 117.13 (C2, C7), 114.10 (C3′, C5′), 108.86 (C8a, C9a), 103.53 (C4, C5), 59.14 (2×CH_2—N(CH_3)$_2$), 44.59 (4×CH_3), 40.73 (2×CH_3′), 37.07 (2×CH_2—NH).

*2.2.14. Synthesis of 3,6-bis[3-(2-dimethylaminoethyl)guanidino]-9-[4′-(N,N-dimethylamino)phenylamino]acridine (**17**)*

Triethylamine (0.5 mL, 3.58 mmol), anhydrous sodium sulfate (1 g, 7.04 mmol), calcium chloride (0.05 g, 0.45 mmol), mercury(II) oxide (0.12 g, 0.58 mmol), and ammonium hydrogencarbonate (0.25 g, 3.16 mmol) were added to the bisthiourea **15** (0.05 g, 0.08 mmol) in 10 mL of methanol with dosing intervals of 5 min for each reactant. The reaction mixture was refluxed for 1 h. An insoluble residue was filtered off and a crude product **17** was purified by column chromatography on silica gel eluted by a methanol–25% water solution of ammonia (50:4).

Yield: 35%, light red solid, mp: 148–149 °C. Anal. Calcd for $C_{31}H_{43}N_{11}$ (569.75): 65.35% C, 7.61% H, 27.04% N. Found: 65.50% C, 7.69% H, 26.99% N. ^{1}H NMR (600 MHz, CD_3OD): 7.82 (d, 2H, H-1,8, J = 9.60), 7.16 (d, 2H, H-4,5, J = 1.80), 6.83 (d, 2H, H-2′,6′, J = 9.00), 6.75 (dd, 2H, H-2,7, J_1 = 2.40, J_2 = 7.20), 6.71 (d, 2H, H-3′,5′, J = 9.00), 3.29 (t, 4H, 2×CH_2—NH, J = 6.00), 2.80 (s, 6H, 2×CH_3′), 2.47 (t, 4H, 2×CH_2—N(CH_3)$_2$, J = 6.60), 2.21 (s, 12H, 4×CH_3). ^{13}C NMR (150 MHz, CD_3OD): 156.00 (2×C═NH), 153.38 (C9), 150.47 (C4a, C10a), 149.64 (C3, C6), 148.79 (C4′), 138.57 (C1′), 127.22 (C1, C8), 122.95 (C2′, C6′), 122.50 (C2, C7), 115.97 (C3′, C5′), 115.89 (C4, C5), 114.69 (C8a, C9a), 59.67 (2×CH_2—N(CH_3)$_2$), 45.50 (4×CH_3), 41.88 (2×CH_3′), 40.13 (2×CH_2—NH).

*2.2.15. Synthesis of 3,6-bis[3-(2-dimethylaminoethyl)-2-methylguanidino]-9-[4′-(N,N-dimethylamino)phenylamino]acridine (**18**)*

Triethylamine (0.5 mL, 3.58 mmol), anhydrous sodium sulfate (1 g, 7.04 mmol), calcium chloride (0.05 g, 0.45 mmol), mercury(II) oxide (0.12 g, 0.58 mmol), and methylamine hydrochloride (0.2 g, 2.09 mmol) were added to the bisthiourea **15** (0.05 g, 0.08 mmol) in 10 mL of methanol with dosing intervals of 5 min for each reactant. The reaction mixture was refluxed for 1 h. An insoluble residue was filtered off and a crude product **18** was purified by column chromatography on silica gel eluted by a methanol–25% water solution of ammonia (50:4).

Yield: 25%, light red solid, mp: 133–135 °C. Anal. Calcd for $C_{33}H_{47}N_{11}$ (597.80): 66.30% C, 7.92% H, 25.77% N. Found: 66.22% C, 7.83% H, 25.70% N. ^{1}H NMR (600 MHz, CD_3OD): 8.25 (d, 2H, H-1,8, J = 9.00), 8.15 (d, 2H, H-4,5, J = 8.40), 7.03 (m, 6H, H-2,7, H-2′,6′, H-3′,5′), 3.64 (s, 6H, 2×CH_3′), 3.35 (t, 4H, 2×CH_2—NH, J = 6.60), 2.83 (s, 6H, 2×CH_3—N═C), 2.54 (t, 4H, 2×CH_2—N(CH_3)$_2$, J = 6.60), 2.29 (s, 12H, 4×CH_3). ^{13}C NMR (150 MHz, CD_3OD): 157.86 (2×CN—CH_3), 157.05 (C9), 156.73 (C4′), 149.75 (C4a, C10a), 144.55 (C3, C6), 141.53 (C1′), 127.19 (C1, C8), 125.91 (C4, C5), 122.73 (C2, C7), 122.03 (C3′, C5′), 109.35 (C2′, C6′), 108.76 (C8a, C9a), 60.09 (2×CH_2—N—(CH_3)$_2$), 45.52 (4×CH_3), 40.81 (2×CH_2—NH), 36.38 (2×CH_3′), 28.97 (2×CH_3—N═C).

*2.2.16. Synthesis of 4-(acetylamino)-2-{[3-(acetylamino)phenyl]amino}-N-benzyl benzamide (**22**)*

A mixture of the acid **7** (1 g, 3.05 mmol) and carbodiimidazole (1.5 g, 9.15 mmol) in dimethylformamide (10 mL) was stirred at room temperature. After the reaction was completed (approximately 2 h, checked by TLC using a mobile phase methanol–ethyl acetate (6:1 v/v)), benzylamine (1 mL, 9.51 mmol) was added. The resultant mixture was stirred at room temperature for 24 h and subsequently poured into distilled water. A precipitated crude product **19** was filtered off and dried on air overnight. The product **19** was purified by column chromatography using a mobile phase methanol–ethyl acetate (6:1 v/v).

Yield: 62%, gray solid, mp: 214–216 °C. Anal. Calcd for $C_{24}H_{24}N_4O_3$ (416.47): 69.21% C, 5.81% H, 13.45% N. Found: 69.33% C, 5.60% H, 13.23% N. ^{1}H NMR (600 MHz, DMSO–D_6): 10.01 (s, 1H, NH′), 10.00 (s, 1H, Ph—NH—Ph), 9.90 (s, 1H, NH″), 9.00 (t, 1H, NH, J = 6.00), 7.69 (d, 1H, H-6, J = 8.40), 7.54 (s, 1H, H-3), 7.41 (s, 1H, H-2″), 7.33–7.32 (m, 4H, H-2‴,6‴, H-3‴,5‴), 7.25–7.21 (m, 3H, H-4‴, H-4″, H-5″), 7.13 (d, 1H, H-5, J = 8.40), 6.88–6.86 (m, 1H, H-6″), 4.45 (d, 2H, CH_2, J = 6.00), 2.03 (s, 3H, CH_3′), 2.01 (s, 3H, CH_3″). ^{13}C NMR (150 MHz, DMSO–D_6): 168.69 (C═O′), 168.54 (C═O), 168.31 (C═O″), 145.66 (C2), 142.69 (C4), 141.60 (C1″), 140.45 (C3″), 139.62 (C1‴), 129.52 (C6, C5″), 128.31 (C3‴, C5‴), 127.24 (C2‴, C6‴), 126.75 (C4‴), 114.37 (C6″), 112.81 (C4″), 112.38 (C1), 110.70 (C2″), 108.67 (C5), 104.21 (C3), 42.39 (CH_2), 24.18 (CH_3″), 24.11 (CH_3′).

2.3. UV–vis absorption and fluorescence measurement

UV–vis absorption spectra were measured on a Varian Cary 100 UV–vis spectrophotometer equipped with a thermostat cell compartment using quartz cuvettes with 1 cm path lengths in a 0.01 M Tris buffer (pH 7.4). The concentration of ctDNA (Sigma Chemical Co.) ranged from 0 to 2.1×10^{-5} M bp. The BRACO19

derivatives were all dissolved in DMSO from which working solutions were prepared by dilution using 0.01 M Tris buffer to a concentration of 2.5×10^{-5} M. All measurements were performed at 25 °C.

UV–vis absorption titrations were performed by the gradual addition of quadruplex DNA solution (0–1×10^{-6} M) to a cell containing a stock solution of studied derivatives (25×10^{-6} M). The spectra were recorded in the 230–600 nm range at 25 °C. All titration experiments were performed in a buffer solution containing 0.01 M Tris–HCl with 50×10^{-3} M KCl, pH 7.4.

Fluorescence measurements were scanned on a Varian Cary Eclipse spectrofluorimeter with a 10 nm slit width for excitation and emission beams. Emission spectra were recorded in the region of 400–750 nm using an excitation wavelength from 371 to 400 nm. Fluorescence titrations were conducted by adding increasing amounts of ctDNA directly into the cell containing the solution of BRACO19 derivatives ($c = 14 \times 10^{-6}$ M, 0.01 M Tris buffer, pH 7.4). The concentration range of DNA was 0–38×10^{-6} M bp. All measurements were performed at 25 °C.

2.4. CD and LD spectroscopy

Prior to use, quadrupled nucleic acid solutions at a final concentration of 15 μM were dissolved in a Tris buffer (pH 7.4) containing 50 mM KCl, which was preheated at 90 °C for 5 min and slowly cooled to room temperature.

CD spectra were recorded on a Jasco J-810 spectropolarimeter in 1 mm quartz cuvettes and are the mean result of three scans from which the buffer background had been electronically subtracted. All measurements were performed in the range of 230–320 nm (450 nm for ctDNA) in a 0.01 M Tris buffer (pH 7.4) at a temperature of 25 °C. The concentration of ctDNA was 4.74×10^{-4} M, the concentration of single strand DNA was 3.5×10^{-5} M, and the concentration of quadruplex DNA was 15×10^{-6} M. The compounds were dissolved in DMSO and titrated into the DNA samples; where appropriate, the sample also contained 50 mM KCl. The concentration of derivatives **13** & **15**–**18** was 0–1.25×10^{-4} M for ctDNA, 0–1.92×10^{-4} M for single strand DNA, and 0–7.30×10^{-5} M for quadruplex DNA.

Flow LD spectra were collected by using a flow Couette cell in a Jasco J-720 spectropolarimeter adapted for LD measurements. All measurements were performed in the range of 210–550 nm, in a 0.01 M Tris buffer (pH 7.4) at a temperature of 25 °C. Long molecules, such as DNA (with a minimum length of 250 bp), can be orientated in a flow Couette cell. The flow cell consists of a fixed outer cylinder and a rotating solid quartz inner cylinder, separated by a gap of 0.5 mm, giving a total pathlength of 1 mm. A water baseline was subtracted from each sample spectrum and the data zeroed at 600 nm. LD spectra were measured at a concentration of 3.1×10^{-4} M of ctDNA and 0–5.7×10^{-5} M of the derivatives **13** & **15**–**18**.

2.5. Viscosimetric titration

The relative viscosity of ctDNA solutions at a concentration of 3.1×10^{-4} M in the presence of derivatives **13** & **15**–**18** (0–46×10^{-6} M) was measured with a micro-viscosimeter (AMVn Automated Micro Viscometer, Anton Paar GmbH, Austria) using a 1.6 mm capillary tube at 25 °C. The density of the solutions was measured with Density Meter DMA 4500 (Anton Paar GmbH, Austria).

2.6. Isolation and cultivation of human fibroblasts

Human fibroblasts were isolated from skin biopsy during abdominal surgery and placed into the transport medium containing phosphate-buffered saline solution (PBS) (GIBCO BRL, Life Technologies, Carlsbad, CA) supplemented with 1% (v/v) antibiotic/antimycotic solution (10,000 units mL^{-1} penicillin, 10,000 μg mL^{-1} streptomycin, and 25 μg mL^{-1} amphotericin B; GIBCO BRL). The experiments were performed with the approval of the University's ethical committee. Epidermis was dissected from skin biopsy and dermis was cut into 2–3 mm^2 pieces and digested with 0.1% (v/v) bacterial collagenase type II (GIBCO BRL) at 37 °C for 6 h. The dermis pieces were filtered through a 40 μm cell strainer (Falcon, BD Biosciences, San Diego, CA) and the filtrate was centrifuged at 300*g* for 7 min. The cells were cultured in 25 cm^2 tissue culture flasks (Sarstedt, Germany) at 37 °C with 5% CO_2 in Dulbecco's modified Eagle's medium (D MEM) (Biochrom AG, Berlin, Germany) containing 1% (v/v) antibiotic/antimycotic solution and supplemented with 10% (v/v) foetal bovine serum (FBS) (GIBCO BRL). When the cells reached 80–90% confluence, they were washed with DMEM medium (Biochrom AG, Berlin, Germany) and detached by incubation with Trypsin–EDTA (GIBCO BRL) for 5 min, washed twice with DMEM (Biochrom AG, Berlin, Germany) and resuspended in culture medium at a density of 2.7×10^5 cells in 75 cm^2 tissue culture flask (Sarstedt, Germany). The cells were passaged every 14–17 day. In the present study, fibroblasts at passage 5 were used for experiments.

2.7. Immunophenotype characterization of human fibroblasts

Immunophenotype characterization of dermal fibroblasts was performed by flow cytometry. After dissociation with Trypsin–EDTA (GIBCO BRL), the cells were washed twice with PBS buffer (GIBCO BRL, Life Technologies, Carlsbad, CA) supplemented with 2% (v/v) FBS. Aliquots of 2.0×10^5 cells were incubated with mouse anti-human CD90/FITC, CD105/PE, CD73/APC, CD26/PE, CD146/FITC and with cocktail of hematopoietic markers: CD14-/CD20-/CD34-/CD45/PerCP. (Miltenyi Biotec GmbH, Bergisch Gladbach, Germany) for 10 min, washed with 1–2 mL of PBS buffer and centrifuge at 300*g* for 10 min. Resuspended cell pellet was analyzed in a Becton Dickinson FACSCalibur using CellQuest software (Becton Dickinson).

2.8. Cell culture conditions

HCT-116 cells. For the experiments, wild type p53 (wt-p53) expressing colon adenocarcinoma-derived HCT-116 cells (ATCC # CCL-247) were cultured in McCoy's 5A medium (Sigma–Aldrich). The cultivation media were supplemented with 10% foetal calf serum and antibiotics (penicillin 100 U mL^{-1}, streptomycin 100 μg mL^{-1}, and amphotericin 25 μg mL^{-1}; Gibco Invitrogen Corp.). The cultures were maintained at 37 °C/5% CO_2/95% humidity. For the experiments, cells were seeded in Petri dishes (TPP, Switzerland). Tested drugs were added to the medium shortly after cell seeding.

2.9. Cell viability assay

HT-29 cancer cells and human fibroblast cells. Adherent cells were trypsinized and seeded in 96-well cell culture plate (10,000/cm^2) (HT-29) and 24-well culture plate (25,000/cm^2) (fibroblasts) in a total volume of 100 (HT-29)/500 (fibroblasts) μL. Cells were allowed to attach overnight and then were treated with studied compounds in varying concentrations dissolved in additional 100 (HT-29)/200 (fibroblasts) μL of culture medium to obtain a total volume of 200 (HT-29)/700 (fibroblasts) μL per well. After 72 or 96 h (HT-29) and 96 h (fibroblasts), 20/70 μL resazurin (final concentration 40×10^{-6} M) was added to each well and the plates were incubated at 37 °C for 1 h. Fluorescence was measured on a FLUOStar Optima (BMG Labtechnologies GmbH, Offenburg,

Germany) using an excitation wavelength of 544 nm and an emission wavelength of 590 nm. Three independent experiments were analyzed in triplicates.

2.10. Cellular proliferation and viability

HCT-116. Cell counts and viability were established using a standard Bürker chamber-based cell count method with eosin staining for viability assessment. In order to test the long term antiproliferative and/or cytotoxic effects of derivatives **13** & **15–18**, a one month long cultivation with repeated cell passage (2-times per week) using one equal concentration (2×10^{-6}) was carried out for all of the tested derivatives. The cells were maintained using a standard cell culturing method: cells were released from adherence by trypsinization, counted and seeded at identical densities each time (9 times).

2.11. Cell cycle analysis

In order to perform flow cytometric analysis of the cell cycle, floating and adherent cells were harvested at intervals of 24, 48, 72, and 96 h after treatment, washed in cold PBS, fixed in cold 70% ethanol and stored overnight at −20 °C. Prior to analysis, cells were washed twice in PBS, resuspended in staining solution (0.1% Triton X-100, 0.137 mg mL^{-1} ribonuclease A, and 0.02 mg mL^{-1} propidium iodide), incubated in darkness at room temperature (RT) for 30 min and analyzed using a FACSCalibur flow cytometer (Becton Dickinson, San Jose, CA, USA). ModFit 3.0 (Verity Software House, Topsham, USA) software was used to generate DNA content frequency histograms and quantify the number of cells in the individual cell cycle phases.

2.12. Statistical analysis

Results were calculated as mean ± standard deviation (SD) of at least three independent experiments. Statistical significance was determined by *t*-test and results were deemed significant if $p < 0.01$ and $p < 0.001$.

2.13. Molecular modeling

Molecular models of acridine ligands were built using the building options of Gabedit [25] package and Chemaxon was used to determine the charge of ligands at physiological pH. All calculations were carried out in NAMD 2.6 using TIP3P potential for waters, parm99.dat parameters set for nucleic acids, and GAFF atom types for the ligand [26–30]. ANTECHAMBER and XLEAP modules of AMBERTOOLS 1.0 software package were applied to extrapolate missing ligand force-field parameters and derive charges using AM1-BCC method. Docking simulations were carried out using AUTODOCK program ver. 4.0, while MGL TOOLS 1.4.3 was used to prepare the input files [31–33]. The X-ray crystal structure of a complex between a bimolecular human telomeric G-quadruplex of sequence d(TAGGGTTAGGGT) and the BRACO19 molecule (PDB: 3CE5) was used as a DNA quadruplex binding model [34]. The PDB coordinates file was imported into Chimera package [35]. The potassium ion and all molecules of water forming interaction network were preserved omitting the ligand molecule to form an interaction cavity for an initial docking of novel braco like structures.

Trajectories were examined visually using VMD 1.8.6 and Chimera software packages [36]. RMSD was calculated between the coordinates of BRACO19 anchor and an identical set of atoms in related structures **13** & **15–18** after 1 ns full production run of binding complex ligand–quadruplex. The BRACO19 anchor is defined as 3,6-diamino-9-[4′-(*N*,*N*-dimethylamino)phenylamino]acridine. For more details see Supporting Information.

2.13.1. Docking studies

The following docking studies were performed in order to ascertain a ligand position and orientation: firstly, the ligand was manually docked into the DNA cavity to form an interaction pose. Docking simulations were carried out using AUTODOCK program ver. 4.0, while MGL TOOLS 1.4.3 was used to prepare the input files. United atom representations for the ligand and DNA were used. Gasteiger partial atomic charges for the ligand and DNA were added. The grid for energy was set in the center of the ligand with dimensions of 60 points × 60 points × 60 points and a spacing of 0.375 Å. Docking runs were performed using Larmarckian genetic algorithm. Docking began with a population of random ligand conformations in a random orientation and at a random translation. Each docking experiment was derived from 200 different runs that were set to terminate after a maximum of 2,500,000 energy evaluations or 27,000 generations, yielding 200 docked conformations. The population size was set to 150. For other parameters, the default values were used. Coordinates from docking studies were used as input coordinates for the following molecular dynamics simulations.

2.13.2. Molecular dynamics (MD) simulations

All calculations were carried out in NAMD 2.6 using TIP3P potential for waters, parm99.dat parameters set for nucleic acids, and GAFF atom types for the ligand. ANTECHAMBER and XLEAP modules of AMBERTOOLS 1.0 software package were applied to extrapolate missing ligand force-field parameters and derive charges using AM1-BCC method.

The results of docking runs were analyzed using MGL TOOLS 1.4.3 software. The ligand pose with the lowest binding energy of the largest docking cluster was chosen as the final ligand orientation. Nonpolar hydrogens were added and the ligand coordinates were extracted as input parameters for construction of DNA–ligand interaction complexes in the following molecular dynamics simulations. In the first step, the DNA quadruplex–ligand complex was solvated in a water-box, dimensions of which were extended to a distance of at least 10 Å from any solute atom. Sodium counterions were then added throughout the cell at grid points of negative coulombic potential using the XLEAP module in order to achieve complete neutralization. Periodic boundary conditions were applied with the particle-mesh Ewans (PME) method, used to treat long-range electrostatic interactions. MD simulations consisted of 1000 steps of minimization followed by 20 ps equilibrations with constrained solute, and subsequently, 1000 steps of minimization with 200 ps equilibrations for the entire system. Finally, a full 1 ns MD production run was performed. The process was carried out for each ligand and ligand free DNA telomeric quadruplex complex. Energy information, averages, and coordinates were recorded every 200 steps and the non-bonded list was updated every 10 steps. Trajectories were examined visually using VMD 1.8.6 software package.

3. Results and discussion

3.1. Molecular dynamics simulations

A molecular modeling approach was adopted in order to compare the interactions between the human telomeric DNA G-quadruplex and the trisubstituted acridines discussed in this paper. A crystal structure of a complex between BRACO19 and the bimolecular human telomeric quadruplex was chosen as a binding model [34], as this model shows a close structural proximity to all of the proposed structures. The network of water molecules which

participate in intermolecular interactions between the ligand and the negatively charged phosphate backbone was also retained in the model for the same reason.

An initial geometry of intended ligand structures within corresponding qDNA complex was obtained by a AUTODOCK software, that was previously successfully applied for various qDNA motives [37–41]. Molecular dynamics simulations were undertaken using NAMD software within an AMBER force field, previously used for an elucidating of qDNA [41–43]. The binding energy of each complex has been calculated and is listed in the Supporting Information. The binding affinity of the proposed structures is shown in Table SP1. The results of the molecular dynamics simulations revealed that all of the proposed compounds would stabilize the binding complex during a 1 ns simulation run. Based on these findings, a series of "braco"-like structures linked at positions 3 and 6 with side chains bearing heteroatomic groups were prepared and studied.

3.2. Synthesis of BRACO19 derivatives

The key step in the preparation of 3,6,9-trisubstituted acridine derivatives was the utilization of the Ullmann-Jourdan reaction. The starting material was 4-amino-2-chlorotoluene (**4**) and 3-aminoacetanilide (**3**). Previous attempts to prepare 3-aminoacetanilide (**3**) through an acylation of phenylenediamine had proven to be ineffective, so the more practical synthetic strategy was an acylation of 4-nitroaniline (**1**) with a subsequent reduction of nitro group was used. However, the use of $SnCl_2{\cdot}2H_2O$ as a reduction agent in hydrochloride or acetic acid led to the deprotection of acetyl group.

The solution was to apply sodium borohydride as a reduction agent using 10% palladium on activated coal as a catalyst (Scheme 1). 4-(Acetylamino)-2-chlorobenzoic acid (**6**) was obtained with a yield of 65% by the oxidation of 4-acetamido-2-chlorotoluene (**5**) with $KMnO_4$ (Scheme 2). Derivative **5** was obtained by the reaction of acetylchloride with 4-amino-2-chlorotoluene (**4**). Substituted diphenylamino carboxylic acid **7** was synthesized through the coupling of 4-(acetylamino)-2-chlorobenzoic acid (**6**) with 3-aminoacetanilide (**3**) in ethoxyethanol with a catalytic amount of copper and copper(I)oxide at reflux.

The next stage of the process was a condensation of diphenylamino carboxylic acid **7** leading to the production of acridones. The structure of carboxylic acid **7** suggests that cyclization would result in two regioisomers, 1,6- and 3,6-substituted acridones (Scheme 3). We therefore decided to develop reaction conditions which would result in a predominance of the 3,6-isomer. As can be seen in Table 1, polyphosphoric (PPA) and sulfuric acid (SA) were used as condensation reagents. In the case of PPA, the best achieved ratio was 2:3 in favor of the 3,6 isomer, but the use of SA resulted in a ratio of 1:4. A further attempt to simplify the cyclization of the substituted diphenylamino carboxylic acid **7** using phosphorus trichloride to obtain a related 9-chloro derivative directly was unsuccessful due to a decomposition of the reactant **7**. Phosphorus trichloride was substituted with thionyl chloride, and the reaction proceeded smoothly for 24 h resulting in a mixture of acridones with predominance of the 3,6-isomer **9a**.

Two different procedures were attempted in order to enhance the solubility of acridones **9a** and **9b** owing to separation. The first method involved an acetylation of the free amino groups, but proved to be unsuccessful. In the second method, butyric anhydride was used and an isomer **10** was separated from hot acetone by filtration (Scheme 4). In a subsequent step, 3,6-bis(butanoylamino)acridone **10** was converted to 3,6-bis(butanoylamino)-9-chloroacridine (**11**) through a reaction with phosphorus trichloride at 70 °C for 1.5 h. The chloro-derivative **11** was purified by crystallization from ethyl acetate.

An initial trisubstituted acridine skeleton **12** was prepared through the reaction of the chloro-derivative **11** with *N,N*-dimethylphenylene-1,4-diamine in phenol at an elevated temperature. The compound obtained through this process, the derivative **12**, was then subjected to sulfuric acid at 100 °C for 15 min to give a free amine **13**, which was then used in the synthesis of a diisothiocyanate **14**. The derivative **14** was subsequently utilized in the preparation of a bisthiourea **15** by the addition of *N,N′*-dimethylethylenediamine to the crude reaction mixture. Owing to a low stability of the diisothiocyanate **14**, its formation was confirmed by the formation of a bisthiourea **15**, clearly characterized by a ^{13}C NMR shift of C=S at 180 ppm.

The bisthiourea **15** was used in the preparation of bisureas **16**, bisguanidines **17** and **18**, bisthiazolidinones **19**, and bisimidazolidinones **20** (Scheme 5 and 6). The bisurea **16** was prepared through the reaction of bisthiourea **15** with mesitylnitrile oxide in methanol for 24 h. Guanidines **17** and **18** were synthetized *in situ* by the addition of ammonium hydrogencarbonate or methylamine hydrochloride to the reaction mixture of thiourea **15** with a desulfurization reagent, HgO, in methanol. The attempted preparation of bisthiazolidinones **19** through the reaction of bisthiourea **15** with methyl bromoacetate was not successful, probably due to a decomposition of the resultant compound. An identical result was obtained in the attempt to synthesize bisimidazolidinones **20**.

An attempt was also made to simplify the reaction pathway toward the trisubstituted acridines by a Bischer-Napieralsky reaction [44] (Scheme 7). As a model compound, an amide **21** prepared by the reaction of aniline and the acid **7** in DMF with an addition of carbodiimidazole was chosen. The reaction of the acid **7** and carbodiimidazole was completed in 2 h leading to the formation of an imidazole amide intermediate. Its subsequent reaction with aniline toward the amide **21** did not proceed; instead, a decomposition at elevated temperature was observed (TLC monitoring). This prompted us to prepare other model amide suitable for an elucidation of the intramolecular cyclization. Thus we decided to substitute aniline by benzylamine what exhibited as a good choice. *N*-Benzyl amide **22** was prepared by the reaction of the imidazole amide intermediate with an excess of benzylamine at room temperature in 24 h; unfortunately, a proposed cyclization of the amide **22** to a final acridine **24** using phosphorus trichloride, sulfuric acid, polyphosphoric acid or thionyl chloride was not possible due to the decomposition of the amide **22**.

3.3. Spectral and DNA binding study

The changes occurring in derivatives **13** & **15–18** following the addition of ctDNA and G-quadruplex DNA (in 0.05 M KCl) were studied using UV–vis spectroscopy. The absorption spectra of the newly synthesized trisubstituted acridine derivatives **13** & **15–18**

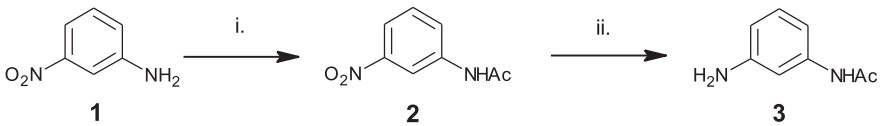

i: acetanhydride, 100 °C, 70%; ii: $NaBH_4$, MeOH, 10% Pd/C, 0 °C, 75%.

Scheme 1.

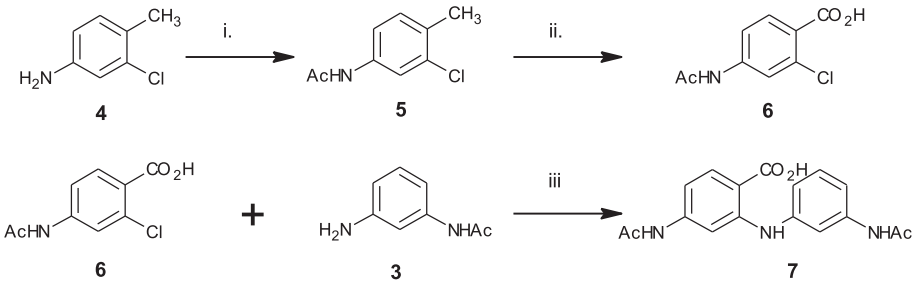

i: CH_3COCl, Et_3N, MC, 95%; ii: $KMnO_4$, H_2O, reflux, 2 h, 65%;
iii: K_2CO_3, Cu, Cu_2O, ethoxyethanol, reflux, 4 h, 50%.

Scheme 2.

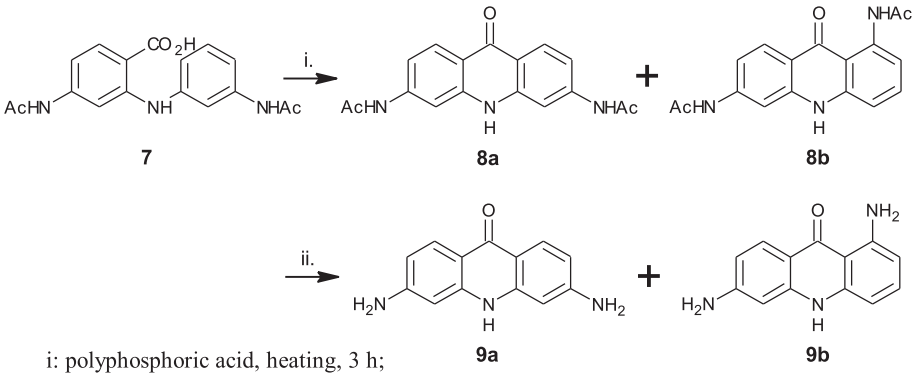

i: polyphosphoric acid, heating, 3 h;
iia: sulfuric acid, 100 °C, 3 h;
iib: thionyl chloride, rt, 24 h.

Scheme 3.

Table 1
Ratios of 1,6- and 3,6-isomeric acridones.

Temperature (°C)	Ratio of acridone isomers			
	PPA		H_2SO_4	
	8a	8b	9a	9b
130	Decomposition		1	1
100	1	1	4	1
80	3	2	No reaction	

in the presence of ctDNA show that all studied derivatives displayed absorption bands in the region of 320–500 nm. The different substituents were found to have an effect on UV–vis spectra, with maximal absorptions of 306–399 nm. It is widely accepted that if the compounds could intercalate DNA, the UV–vis curve of their complexes would demonstrate bathochromic shifts and hypochromicity [45–47]. The absorption spectra of **13** & **15–18** (2.5×10^{-5} M) in both the absence and presence of calf-thymus DNA (0–2.5×10^{-5} M) are given in Fig. SP1. As the concentration of DNA increases, the curve shows significant levels of hypochromicity (20–40%) and a mild bathochromic shift. UV–vis data for compounds **13** & **15–18** with ctDNA are displayed in Table 2, with qDNA in Table 3.

UV–vis absorption titrations can be used to observe the interaction of Braco19 derivatives with DNA. A hyperchromism or hypochromism and shift (red or blue) often occur in absorption spectrum of ligands when the complex is bound to DNA. As the concentration of DNA increases, the curve shows significant levels of hypochromicity and a mild bathochromic shift indicating that the compounds **13** & **15–18** form a complex with DNA. The absence of the tight isosbestic points in the titration experiment indicate that more than one type of DNA–ligand complex could have been formed. Comparing the value of hypochromism in this study with those obtained in our previous research (34–54%) [19], it is possible to suggest less proximity of the acridine chromophore to DNA for our compounds which could be caused by weaker interaction between the electronic states of the chromophore and those of the DNA base (a result, in turn, of different substituents on the acridine chromophore). As the concentration of qDNA increases, the curve shows slight hypochromicity (11.9–35.7%) and a mild bathochromic shift indicating that the compounds form a complex with DNA.

The values of binding constants K were determined by spectrophotometric titration as being in the range of 1.5×10^4 to 8.2×10^3 M^{-1} for ctDNA. Estimates for n lay in the range of 2.0–4.4 bp. The calculated binding constants, K, and the neighboring exclusion parameters, n, clearly indicate a direct link between intercalation capability and structural changes of acridine derivatives **13** & **15–18** and BRACO19. These results prove the low affinity of the acridine ligands to DNA-base pairs and correspond to typical binding constants for intercalation complexes. Typical binding constants for intercalation complexes between organic dyes and ctDNA range from 10^4 to 10^6 M^{-1} and are usually significantly smaller than the binding constants of groove binders (10^5 to 10^9 M^{-1}). Moreover the rate of association/dissociation of intercalators is high [48]. The binding constants of derivatives **13** & **15–18** are also of the same order of magnitude as those found in our previous study [22,49]. Estimates for n lay in the range of 2.0–4.4 bp. The relative binding constants K increased as follows: **17** < **18** < **16** < **13** < **15** < BRACO19. The binding constants for

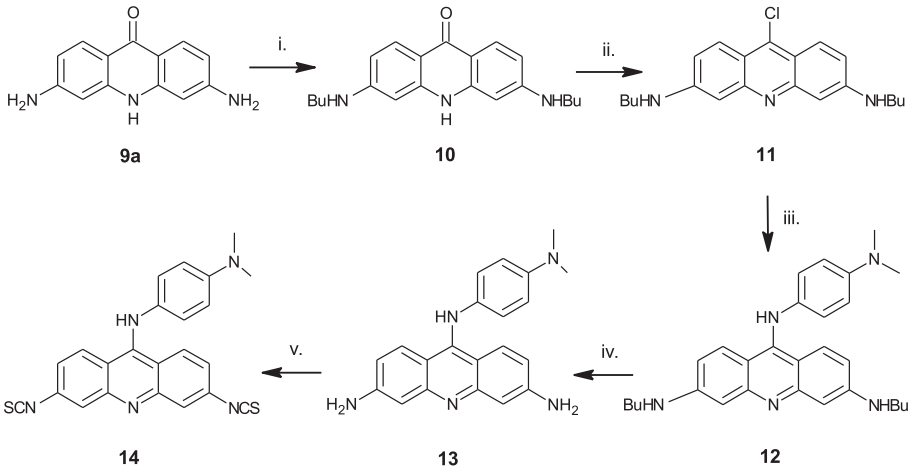

i: $(CH_3CH_2CH_2)_2CO$, 100 °C, 2 h, 55%;
ii: $POCl_3$, 70 °C, 1.5 h, 45%;
iii: phenol, *N,N′*-dimethylbenzene-1,4-diamine, 100 °C, 2 h, 60%;
iv: H_2SO_4, 100 °C, 15 min, 75%;
v: $CSCl_2$, $NaHCO_3$, $CHCl_3$, H_2O, 0 °C, 2 h.

Scheme 4.

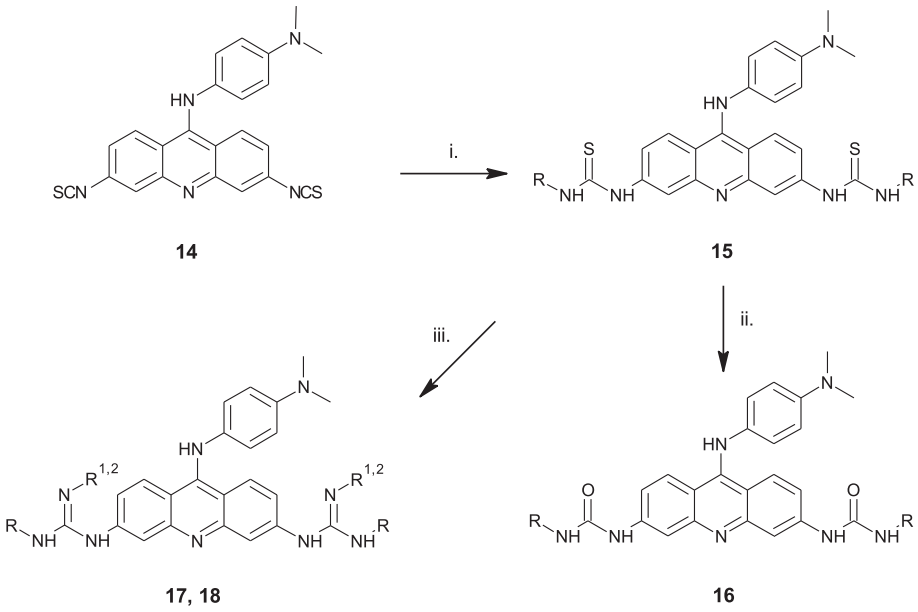

R: $CH_2CH_2N(CH_3)_2$
i: R-NH_2, $CHCl_3$, Et_3N, -20 °C, 1 h, 65% ;
ii: mesitylnitrile oxide, MeOH, rt, overnight, 30%;
iii: R^1=NH_2, NH_4HCO_3, HgO, Na_2SO_4, $CaCl_2$, Et_3N, MeOH, reflux, 1 h, 35%;
R^2=CH_3NH_2, CH_3NH_2.HCl, HgO, Na_2SO_4, $CaCl_2$, Et_3N, MeOH, reflux, 1 h, 25%.

Scheme 5.

G-quadruplexes showed an affinity ten times higher than that of ctDNA (1.2×10^4–4.7×10^5 M^{-1}), which corroborates the findings of Li et al. [49,50] in which the interaction mechanism of Zn-PP with three types of human telomeric G-quadruplex DNA and with ctDNA was studied with UV–vis, fluorescence and CD spectroscopic methods. The results indicated that Zn-PP exhibits a higher binding affinity with human telomeric G-quadruplex DNA than with ctDNA. This might be a result of the more expanded planar aromatic structure of G-quadruplex DNA in comparison to that of ctDNA as this structure is known to facilitate π–π stacking with Zn-PP; the antiparallel G-quadruplex form of DNA is also more stable than the double helix form of DNA in the presence of the studied compounds.

The binding activity of ligands **13** & **16**–**18** with ctDNA was also studied using fluorescence spectroscopy. Our derivatives exhibited a broad emission band in the range of 400–600 nm for **13**, **16** & **17**, and of 420–720 nm for compound **18**. No fluorescence was observed for derivative **15**. The spectra were monitored at a fixed

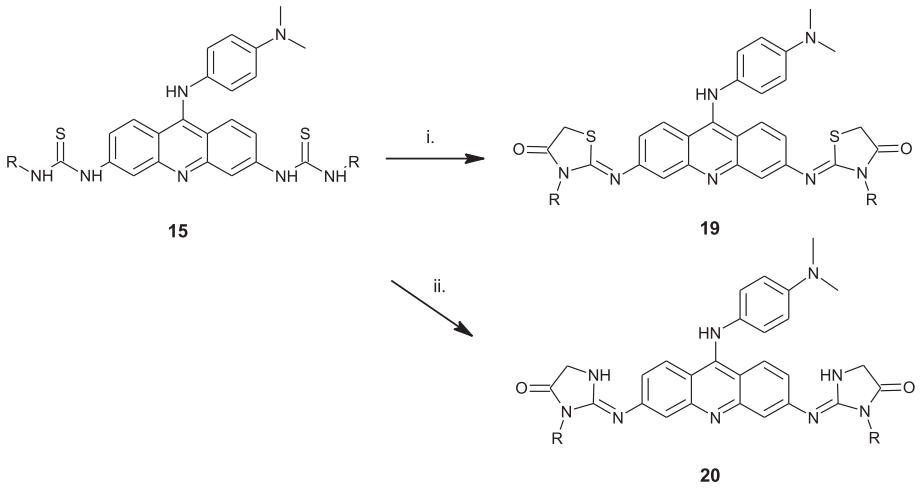

R: $CH_2CH_2N(CH_3)_2$
i : $BrCH_2CO_2CH_3$, Et_3N, MeOH, rt, 1 h;
ii: $NH_2CH_2CO_2CH_2CH_3$.HCl, HgO, Na_2SO_4, $CaCl_2$, Et_3N, MeOH, reflux, 1 h.

Scheme 6.

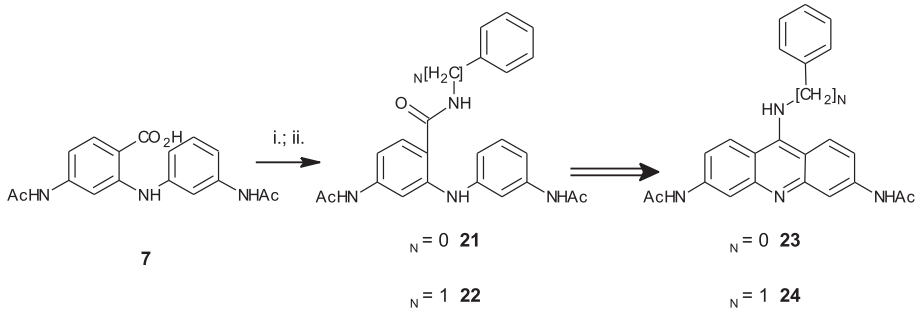

i:carbodiimidazole, DMF, r.t, 2 h
ii:$Ph(CH_2)_NNH_2$, DMF, r.t., 24h, 60%

Scheme 7.

Table 2
UV–vis absorption data of BRACO19 and its derivatives **13** & **15–18** in the presence of ctDNA.

Compound	λ_{max} free (nm)	λ_{max} bond (nm)	$\Delta\lambda$ (nm)	Hypochromicity (%)	K_d (M^{-1})	n
13	399	404	5	20.0	1.7×10^4	2.0
15	373	376	3	40.0	8.2×10^3	3.9
16	380	390	10	27.8	6.5×10^3	3.4
17	375	381	6	26.9	4.8×10^3	3.5
18	372	365	7	38.5	4.7×10^3	4.4
BRACO19	360	362	2	24.3	1.5×10^4	3.8

Table 3
UV–vis absorption data of BRACO19 and its derivatives 13 & 15–18 in the presence of qDNA.

Compound	λ_{max} free (nm)	λ_{max} bond (nm)	$\Delta\lambda$ (nm)	Hypochromicity (%)	K_d (M^{-1})	n
13	400	402	2	14.2	8.6×10^4	1.9
15	373	279	6	23.3	9.2×10^4	3.0
16	377	389	12	15.4	2.9×10^4	3.1
17	371	371	0	11.9	1.2×10^4	2.9
18	359	359	0	15.5	2.3×10^4	3.6
BRACO19	360	366	6	35.7	4.7×10^5	4.5

concentration of ligand to which increasing concentrations of ctDNA were added (Fig. SP2). Derivative **18** demonstrated the highest fluorescence intensity and compound **16** the lowest (Table 4). The decrease in the fluorescence detected for all compounds was quite considerable, as is typical for classical intercalators [51].

CD is a powerful and reliable tool which is used to determine the conformation of biomacromolecules. CD spectra can be used to monitor the asymmetric environment of the compounds when bound to DNA and can therefore also be used to obtain information on the binding mode. The CD spectrum of free ctDNA has a negative band at 245 nm due to helicity, and a positive band at 279 nm due to base stacking which is characteristic of DNA in the right-handed B form [52,53].

When the studied compounds were incubated with ctDNA, the CD spectra displayed changes in both the positive and negative CD bands. Based on obtained results, we can assume that derivative **13** (which has no side-chains) is the only compound among those studied in this paper which intercalates into DNA, whereas the other derivatives bind to DNA using alternative forms of binding. It is possible to suggest that the acridine skeleton was intercalated

Table 4
Fluorescence spectral data of derivatives **13** & **16–18**.

Compound	λ_{ex} (nm)	λ_{em} (nm)	F/F_0[a]
13	400	495	0.28
16	373	419	0.11
17	373	501	0.35
18	371	560	1.00

[a] Relative fluoresce related to fluorescence maximum of 14×10^{-6} M solution of (**18**).

between the base pairs and that the long side chains bind in the groove of DNA.

Circular dichroism (CD) spectroscopy, linear dichroism (LD) and viscosimetry were also used in order to provide a more detailed study of the binding of derivatives **13** & **15–18** and BRACO19 to ctDNA. After incubation of samples with ctDNA, the CD spectra displayed changes in both the positive and negative CD bands (Figs. 1 and SP3). Derivative **13** showed a significant increase in ellipticity in the positive band, an enhancing of the negative signal at 245 nm and also an induction of the negative signal at 350–450 nm, features which are characteristic for intercalators. Similar changes were also observed for derivative **17**. In the presence of derivative **16**, no significant changes were observed in the CD spectrum in the range of 220–300 nm (B-DNA conformation was intact; instead, only a small induction of the positive signal was observed at 325 nm and a negative signal at 375 nm. Similar changes in the range of 300–450 nm were also recorded for derivatives **15** and **18**, although these derivatives disrupted B-DNA conformation which subsequently led to an increase in the positive signal. The induction of the positive signal at 325 nm was also observed for BRACO19.

The LD spectra of ctDNA and ctDNA in the presence of derivatives **13** & **15–18** are given in Figs. 2 and SP4. The results for ctDNA show a characteristic negative peak at 259 nm. In the presence of **13** & **15–18** and BRACO19, there is an increase in the intensity of the negative LD signal when compared to that of ctDNA alone. The DNA LD bands (220–300 nm) confirm that the DNA remains in the B-DNA conformation in the presence of **13** & **15–18** and BRACO19, although some structural changes in DNA are suggested by the increase in the amplitude of DNA negative LD band at 259 nm upon the addition of the compound (Figs. 2 and SP4).

LD, which can be used to probe the orientation of molecules, was also used in order to ascertain the other DNA binding modes of **13** & **15–18** and BRACO19. In the presence of **13** & **15–18** and BRACO19, there is an increase in the intensity of the negative LD signal when compared to that of ctDNA alone. The DNA LD bands confirm that the DNA remains in the B-conformation in the presence of **13** & **15–18** and BRACO19, although some structural changes in DNA are suggested by the increase in the amplitude of DNA negative LD band (Figs. 2 and SP4). An increase in the amplitude of the negative 259 nm LD band of DNA is usually associated with DNA stiffening [54–56] since the aromatic rings of the derivatives are able to insert between base pairs on the DNA thereby making the DNA more rigid and increasing the alignment [57]. Thus, the effect of **13** & **15–18** and BRACO19 on the DNA LD signal is consistent with the intercalative mode of interaction which is typical for all of the "braco"-type derivatives tested in this study.

A number of negative signals were recorded due to the "braco"-type derivatives in the region of ~350–500 nm and others showing as shoulders on the DNA signal at ~300 nm. Compounds **13** & **15–18** and BRACO19 are too small to be orientated and thus show no intrinsic LD signal. Any LD signals which arise in the spectroscopic regions of complexes **13** & **15–18** and BRACO19 in the presence of ctDNA would therefore indicate binding of the complex to ctDNA in a specific orientation or orientations rather than in a random arrangement. Moreover, the LD signals which arise in the region of over 300 nm exhibit the same signals as the DNA bands. This observation is in agreement with a coplanar arrangement of the DNA base pairs and the **13** & **15–18** and BRACO19 moiety, which is highly suggestive of classical intercalative binding. It is also likely that the angle of the long axis of **13** & **15–18** and BRACO19 to the axis of the DNA double helix is more than 54° as is typical for intercalators [54,58].

The LD signals which arise in the spectroscopic regions of the "braco" derivatives in the presence of ctDNA are more variable, which is consistent with the mixed polarization of this transition [59] wherein small angle variations in the binding geometry can lead to signal changes. It is clear from these spectra that the extent of orientation is more significant for derivative **13** than for the other derivatives tested in this study, as can be seen by the reduced intensity of the signal in the spectroscopic regions of derivatives in the presence of ctDNA.

The next goal of the study was to obtain additional data to support the findings on the DNA intercalation binding mode of derivatives **13** & **15–18** which had been inferred from the results of LD spectra. When a ligand inserts itself between adjacent base pairs within duplex DNA, the helix must unwind to create a gap in order to accommodate the incoming ligand. This unwinding process increases the overall contour length of the helix and, as a result, the DNA solution becomes more viscous, and measurement of this viscosity is regularly used as a simple method for determining the binding modes of DNA ligands [54]. Because groove binding compounds do not require insertion between the base pairs, DNA lengthening does not occur, and the viscosity of the solution is not significantly altered. Viscosimetric experiments can therefore be readily employed to distinguish between different non-covalent DNA binding modes.

Our viscosity data (Fig. 3) demonstrate that compounds **13** & **15–18** and BRACO19 caused a significant increase in the viscosity of the DNA solution, with derivative **13** proving the most effective. The results illustrate the lengthening of DNA indicating the intercalation of **13** & **15–18** and BRACO19. The higher rate of intercalation observed for compound **13** is consistent with the most significant extent of orientation of derivatives **13** & **15–18** interacting with DNA which was inferred from the results of LD spectra (Fig. 3).

This increase in viscosity is due to the increase in separation of base pairs at intercalation sites, which results in an increase in overall DNA contour length [60,61]. Thus, the results illustrate the lengthening of DNA indicating the intercalation of **13** & **15–18** and BRACO19. The higher rate of intercalation observed for compound **13** is consistent with the most significant extent of orientation of derivatives **13** & **15–18** interacting with DNA which was inferred from the results of LD spectra.

Human telomeric DNA in the absence of salt exists in an unfolded single-stranded structure. In Figs. 4 and SP5, it can be seen that the addition of BRACO19 and its derivatives **13** & **15–18** to a solution of single-stranded DNA leads to significant changes in the CD spectra of the DNA; in particular a decrease or even a total disappearance of the positive and negative signals and a subsequent induction of new signals (positive at 295 nm and negative at about 260 nm).

The interaction of the derivatives with human telomeric DNA was also studied in a medium containing K^+ ions. As is depicted in Figs. 5 and SP6 with a black line, the CD spectra obtained in the absence of ligand show a main positive signal at 290 nm with a strong peak at a wavelength of about 270 nm and a smaller negative peak at around 235 nm, spectral characteristics which are typical for a quadruplex stabilized with potassium ions (hybrid type) [62]. After the addition of derivatives **13** & **15–18** (blue, green, red line, respectively) a number of changes were observed

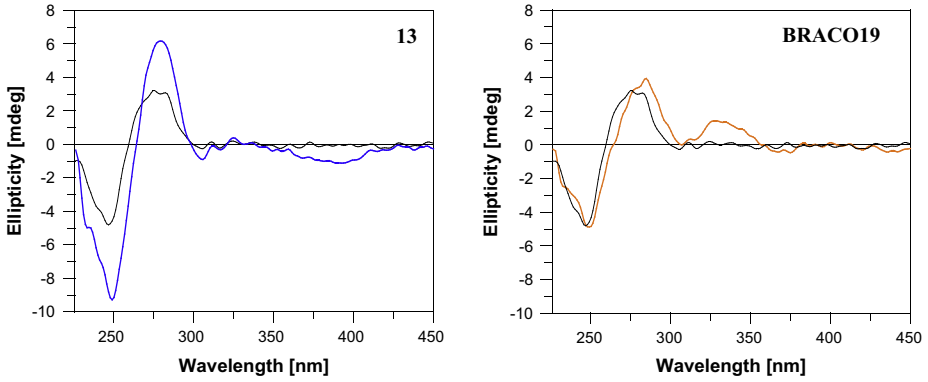

Fig. 1. CD spectra of ctDNA (black line, 4.74×10^{-4} M) in the presence of derivatives **13** and BRACO19 (0–1.25×10^{-4} M) in 0.01 M Tris–HCl buffer, pH 7.4.

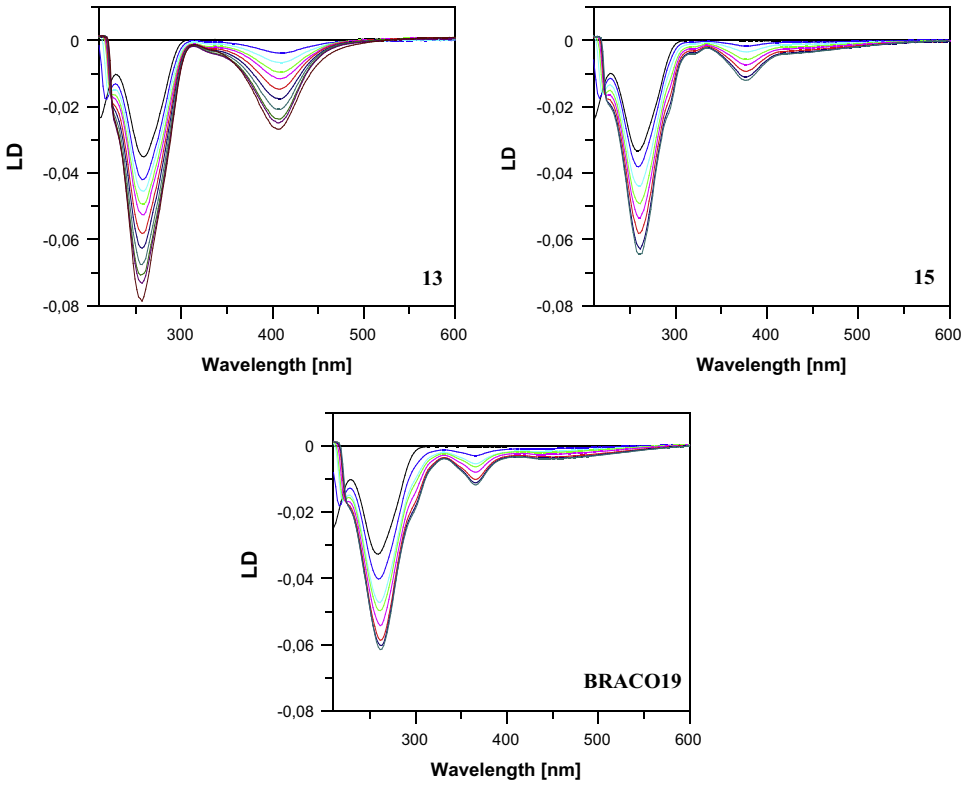

Fig. 2. Linear dichroism (LD) spectra of ctDNA (3.11×10^{-4} M) in the presence of increasing amounts of **13**, **15** and BRACO19 (0–75.7×10^{-6} M) in 0.01 M Tris–HCl solution, pH 7.4.

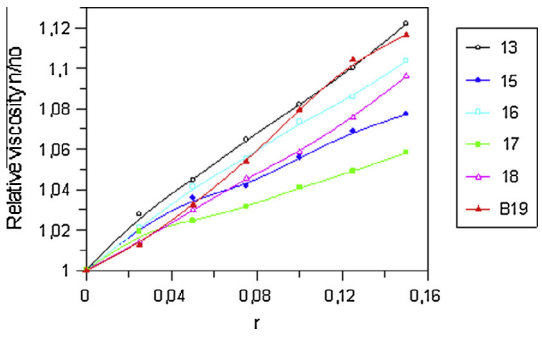

Fig. 3. Effect of increasing amounts of derivatives **13** & **15–18** and BRACO19 (0–46×10^{-6} M) on viscosity of ctDNA (3.11×10^{-4} M) in 0.01 M Tris–HCl buffer, pH = 7.4.

in the CD spectra. The addition of derivatives **13** & **15–17** led to decreasing ellipticity at 270 nm, a deepening of the peak at 260 nm, the induction of the CD signal at about 245 nm and increasing (derivative **16** and **17**) or decreasing (derivative **13** & **15**) signals at 295 nm. A slight red shift was also observed for derivative **15**. Similar changes were also recorded after the addition of the positive control BRACO19. The most significant changes were observed after the addition of derivative **16** to the DNA; this addition resulted in increasing ellipticity at 290 nm, the loss of peak at 270 nm, the induction of the negative signal at 260 nm and of the positive signal at 245 nm. No significant changes in the CD spectrum of the DNA were recorded following the addition of derivative **18**, so it can be assumed that this derivative binds with four-stranded DNA either very weakly or not at all.

The initial results of our UV–vis spectroscopy study indicate that some of our new derivatives show evidence of binding to

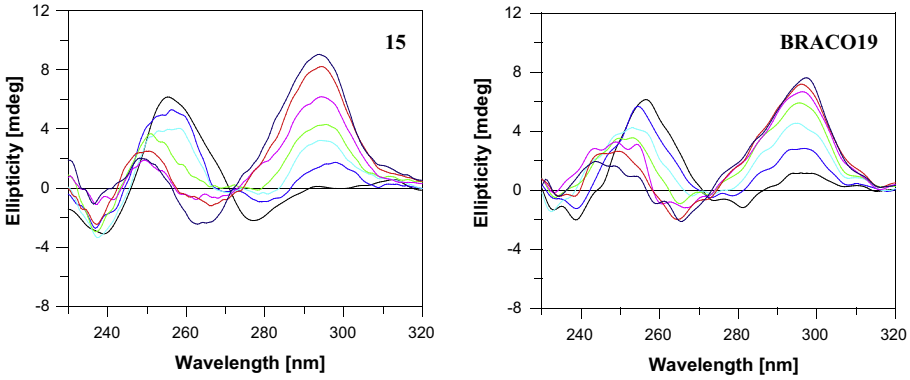

Fig. 4. CD spectra of single stranded DNA (3.5×10^{-5} M) at increasing concentrations of BRACO19 and derivative **15** (0–1.92×10^{-4} M) in 0.01 M Tris–HCl solution, pH 7.4.

qDNA. Based on these findings, we performed further studies in order to determine which ligands are capable of forming and/or stabilizing four stranded DNA and which of them show a higher affinity towards double-stranded DNA. For these experiments, an oligonucleotide with the human telomeric sequence dAGGG $(TTAGGG)_3$ (qDNA) was examined in order to establish the ability of the compounds to form or fold this single-stranded DNA into four-stranded DNA in the absence of ions. The influence of the compounds on the already created G-DNA in the presence of 0.05 M KCl and their ability to stabilize four stranded DNA by using circular dichroism were also studied.

The different structures of DNA each have their own characteristic CD spectral features [62] and these features can be used to distinguish the DNA motifs and to observe the changes in the structure of DNA by its interaction with substances of low molecular weight. Spectra with a positive signal at 260 nm and negative at 240 nm are characteristic of parallel quadruplex structures, while positive peaks at 295 nm and 245 nm and a negative peak at 260 nm are typical for antiparallel structures [63,64].

Human telomeric DNA in the absence of salt exists in an unfolded single-stranded structure which is characterized by CD spectra by a positive signal at 254 nm and a negative signal at 237 nm. The results show that all of the studied derivatives are able to fold single-stranded DNA with human telomere sequences into antiparallel G-quadruplex structures. The smallest change in the CD spectrum was that caused by derivative **13**, which could indicate that this derivative is unable to fold single-stranded structure DNA into G-quadruplexes in the absence of ions. The resulting spectrum induced in the presence of ligands is characteristic of that of antiparallel G-quadruplex structures [62].

After the addition of derivatives **13** & **15**–**18** a number of changes were observed in the CD spectra. On the basis of these measurements, we assume that derivatives **13**, **15** & **17** are capable of stabilizing the antiparallel G-quadruplex form; the least efficient agent was derivative **13**, for which only minimal changes were observed. All of these results are consistent with those of antiparallel forms of the G-quadruplex [63,64], and it is therefore possible to conclude that this derivative can stabilize the antiparallel conformation formations of human telomeric quadruplex DNA. On the basis of these measurements, we can assume that derivatives **13**, **15** & **17** stabilize the antiparallel form of hybrid G-quadruplex in a manner similar to that of compound BRACO19, while derivative **16** is able to form both mixed parallel/antiparallel quadruplexes and entirely antiparallel structures.

3.4. Cellular proliferation and viability

To test the long term anti-proliferative/cytotoxic effects of "braco" derivatives we have executed a one month long cultivation with repeated cell passage (2-times per week) using one equal concentration (2×10^{-6} M) for all tested derivatives. The HCT-116 cells were released from adherence by trypsinization, counted and seeded in the same density each time (9 times). During the experiment period, the HCT-116 cells were allowed to undergo approx. 33-doubling periods (untreated control). To compensate for any fluctuations, we compared the total number of cells that were grown in each experimental group during the testing period (Fig. 6A). As might be seen, only the positive control BRACO19 and **13** derivatives were able to suppress cell proliferation significantly. But even in these two experimental groups, there were no progressive declining trends indicating a falling of the cellular "fitness" (Fig. 6B). Therefore we may presume that the effect was more-less cytostatic at the given concentration. Insignificant effect of 10-times lower BRACO19 concentration (B0.2) supports this conclusion.

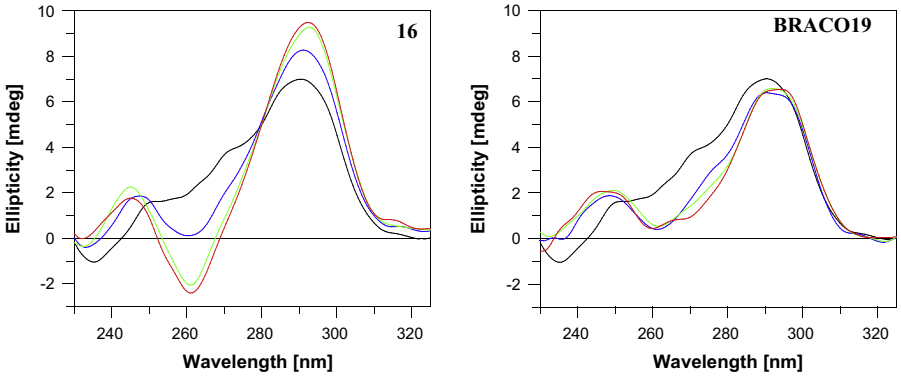

Fig. 5. CD spectra of human telomeric DNA (15×10^{-6} M) in 0.05 M KCl (black line) at increasing concentrations of BRACO19 and derivative **16** (0–7.30×10^{-5} M) in 0.01 M Tris–HCl, pH 7.4.

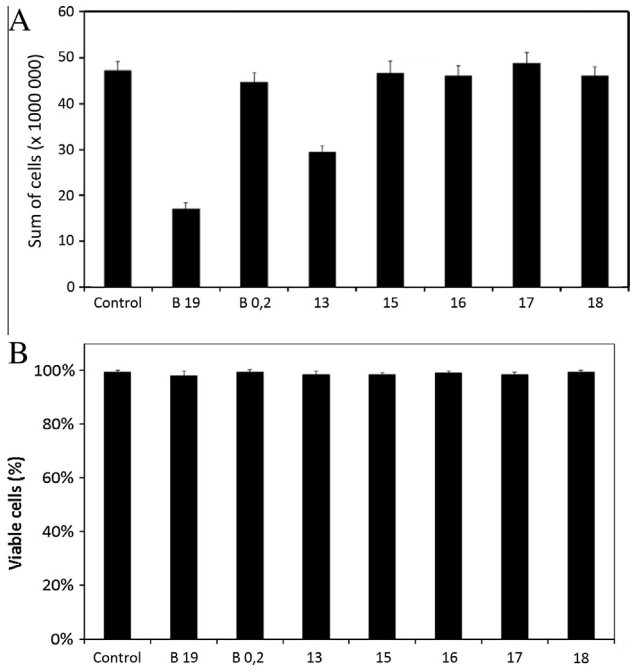

Fig. 6. The number of cells in experiments (A) a viability cells HCT-116 (B) after incubation with studied derivatives **13** & **15–18** after 1 month.

We have also employed adherent cell line HT-29 to test concentration- and time-dependent effect of **13** & **15–18**. Concentrations ranging from 0.1 to 25 × 10^{-6} M (for BRACO19 and **13**) and 1 to 100 × 10^{-6} M (for derivatives **15–18**) were tested for 72 (Fig. 7A) and 96 (Fig. 7B) hours. BRACO19 was used as positive control. The results prove that only derivative **13** is highly effective at lower concentrations (5–25 × 10^{-6} M), while effects of the other derivatives were 2–3 times weaker (Fig. 7). IC_{50} values are given in Table 5.

The cytotoxicity of **Braco 19** (positive control), **13** & **15–18** toward cultured human dermal fibroblasts was also examined. Human fibroblasts were isolated from skin biopsy during abdominal surgery and were characterize by flow cytometry. Flow cytometric analysis showed that human fibroblasts after five passages were positive for CD90 (96.98%), CD105 (87.69%), CD73 (98.65%) and CD26 (95.33%) antigens and negative for cocktail of CD14, CD20, CD34, CD45 (0.29%) and CD146 (0.01%) antigens (Fig. SP7). Concentration of drugs were 15 μM, 25 μM (for **Braco 19** and **13)** and 50 μM, 100 μM (for **15–18)** and cells were incubated for 96 h (Fig. 8A and B). As shown in Fig. 8, all newly synthesized derivatives are less toxic to non-cancer cells as cancer cells.

Cell cycle analysis revealed a primary trend of BRACO19 derivatives to arrest the cells in S- and G_2M-phase of the cell cycle within first 72 h, especially the **13** and BRACO19. These effects might be related to their primary mechanism of action and might be responsible for cytostatic effect. Summing up, we may conclude that only the **13** derivatives demonstrated significant cytostatic–cytotoxic effect with both HCT-116 and HT-29 cell lines.

Having outlined the results of the experimental work, it might be useful to compare these findings with the predictions obtained though the molecular dynamics simulations. The simulations sug-

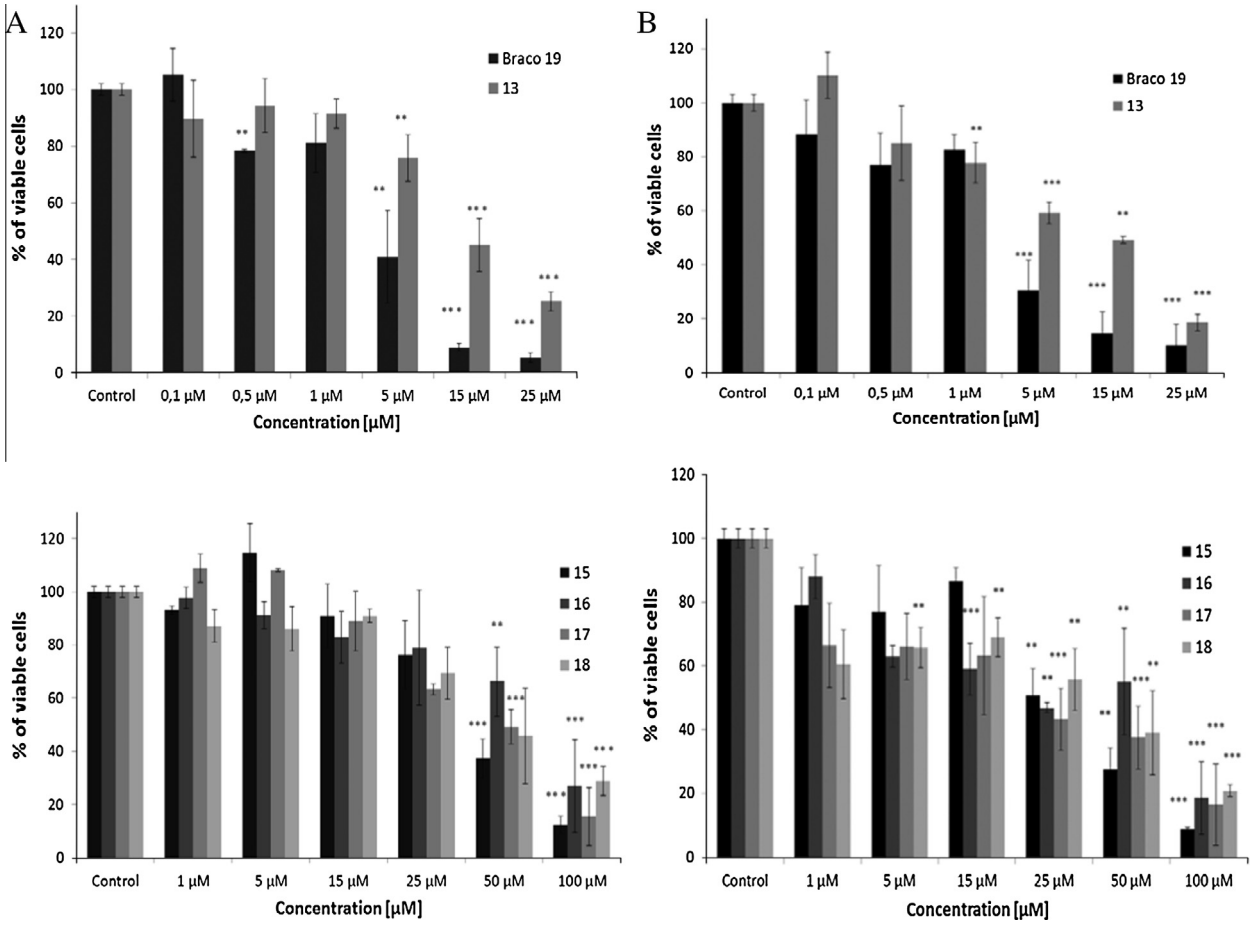

Fig. 7. The viability TH-29 cells treated with different concentrations of derivatives **13** & **15–18** (0, 1–100 × 10^{-6} M) for 72 h (A) and 96 h (B). The results are presented as a mean ± SD, statistical significance: $p < 0.01$ (**), $p < 0.001$ (***) for particular experimental group compared to untreated control.

Table 5
IC_{50} values for viability of HT-29 cells 72 and 96 h after treatment with BRACO19, **13** & **15–18**.

72 (h)	IC_{50} (μM)	96 (h)	IC_{50} (μM)
BRACO19	3.57	BRACO19	3.56
13	13.17	**13**	12.55
15	41.12	**15**	27.38
16	69.99	**16**	22.12
17	48.80	**17**	23.25
18	44.89	**18**	33.23

gested that compounds containing guanidine cores, namely derivatives **17** and **18**, would exhibit superior binding affinity. However, this assumption is contradicted by the experimental findings which show that the thiourea-based derivative **15** possesses the highest DNA quadruplex binding affinity. Interestingly, a relation was also observed between RMSD and the binding constant (Fig. 9). In this connection, it is possible to suggest that compounds with close structural similarities to BRACO19 may possess similar intermolecular forces which can stabilize ligands close to the initial position of BRACO19 within the binding complex. There is possible

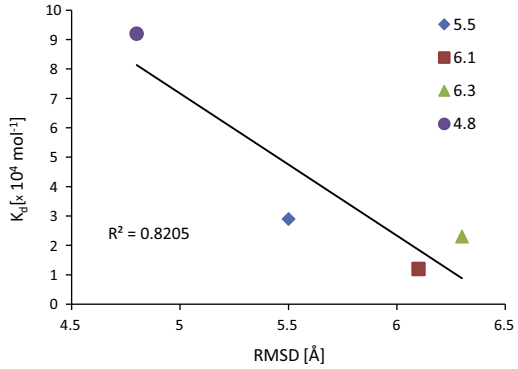

Fig. 9. Plot of calculated relative RMSD *vs* the binding constants of the quadruplex complex with compounds **15**–**18**, from Table SP1.

to conclude that ureido/thioureido moieties of **15** and **16** are more resemble to a weakly basic amido moiety in BRACO19, than guanidino ones of derivatives **17** and **18**, that are protonized at the physiological pH. This might result in a small relative RMSD for

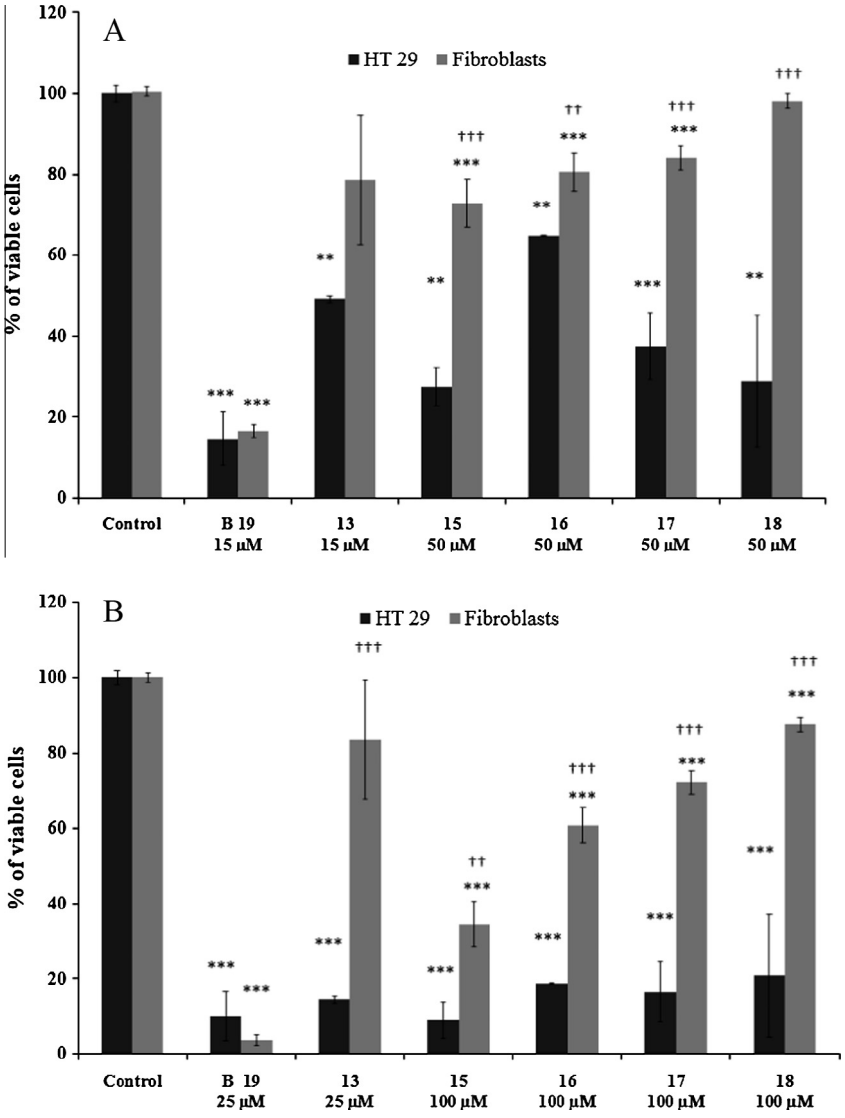

Fig. 8. The viability HT-29 and human fibroblasts cells treated with different concentrations of derivatives **13** & **15–18** (A. 15 (**B19**,**13**) and 50 (**15–18**) × 10^{-6} M and B. 25 (**B19**,**13**), 100 (**15–18**) × 10^{-6} M) for 96 h. The results are presented as a mean ± SD, statistical significance: $p < 0.01$ (∗∗), $p < 0.001$ (∗∗∗) for particular experimental group compared to untreated control (∗) and $p < 0.01$ (††), $p < 0.001$ (†††) for fibroblasts experimental group compared to HT 29 experimental group.

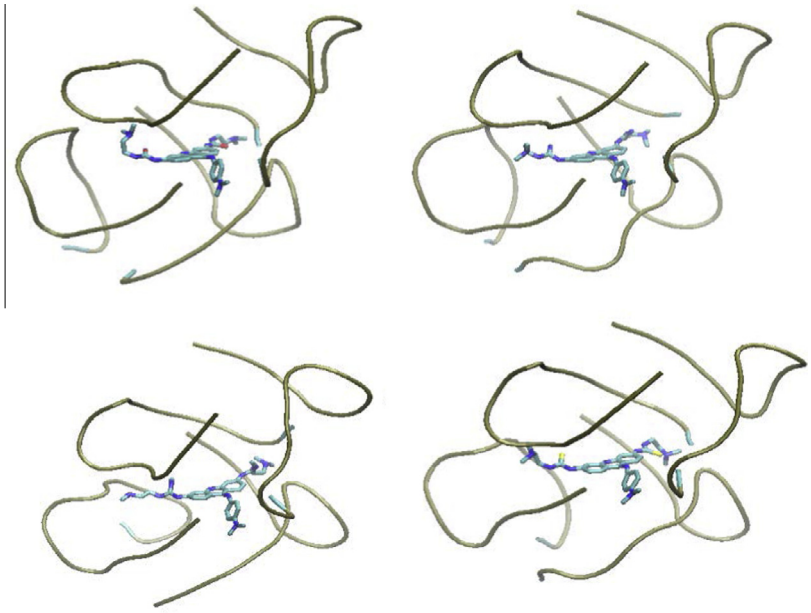

Fig. 10. Putative position of derivate **15**–**18** (from top left to bottom right) after full 1 ns production run within binding DNA quadruplex–ligand complex. All hydrogens are omitted for clarity. Nucleotides are drawn in a tube representation and ligands in a licorice representation.

compounds with the highest levels of interaction with the DNA quadruplex (Fig. 10). However, due to fact that this study is restricted to a relatively limited set of molecules, these findings must be treated with care.

4. Conclusion

New trisubstituted acridines were synthetized that was modified at positions 3 and 6 by thiourea, urea and guanidines. For more detail study of binding to DNA, we used the UV–vis spectroscopy, circular dichroism, linear dichroism and viscosimetry. Based on these results, we assume that among all the studied derivatives only derivative **13** (which has no side-chains) intercalates into DNA, whereas the other derivatives bind to DNA also with another type of binding. The values of binding constants *K*, determined by spectrophotometric titration are in the range of 1.5×10^4 to 8.2×10^3 M^{-1} for ctDNA. The measured results show that all studied derivatives are able to fold the single-stranded DNA with a human telomere sequences in antiparallel G-quadruplex structure with ten times higher affinity to human telomeric DNA quadruplex over DNA duplex. On the basis of these measurements, we can assume that the derivatives **13**,**15**,**17** stabilize antiparallel form of hybrid G-quadruplex similar to drug BRACO19, while derivative **16** is able to form mixed parallel/antiparallel quadruplex and create only antiparallel structure. The derivative **18** didn't change hybrid quadruplex structure and/or is unable to bind with it. Cell cycle analysis revealed a primary trend of "braco" derivatives to arrest the cells in S- and G_2M-phase of the cell cycle within first 72 h, especially the **13** and BRACO19. These effects might be related to their primary mechanism of action and might be responsible for cytostatic effect. Summing up, we may conclude that only the 13 derivatives demonstrated significant cytostatic–cytotoxic effect with both HCT-116 and HT-29 cell lines.

Acknowledgments

This study was supported by Slovak Research and Development Agency under Contract VVCE-0001-07, APVV-0280-11, VEGA Grants Nos. 1/0001/13 and 1/0672/11, Internal Grant Program of the P.J. Šafárik University in Košice (VVGS-PF-2013-78). Molecular graphics images were produced using a UCSF Chimera package from the Resource for Biocomputing, Visualization, and Informatics at the University of California, San Francisco (supported by NIH P41 RR-01081).

Appendix A. Supplementary material

Supplementary data associated with this article can be found, in the online version, at http://dx.doi.org/10.1016/j.bioorg.2014.07.010.

References

[1] S. Burge, G.N. Parkinson, P. Hazel, A.K. Todd, S. Neidle, Nucleic Acids Res. 34 (2006) 5402–5415.
[2] S. Neidle, S. Balasubramanian, Quadruplex Nucleic Acids, Royal Society of Chemistry, Cambridge, UK, 2006.
[3] N.W. Kim, M.A. Piatyszek, K.R. Prowse, C.B. Harley, M.D. West, P.L. Ho, G.M. Coviello, W.E. Wright, S.L. Weinrich, J.W. Shay, Science 266 (1994) 2011–2015.
[4] W.C. Hahn, S.A. Stewart, M.W. Brooks, S.G. York, E. Eaton, A. Kurachi, R.L. Beijersbergen, J.H.M. Knoll, M. Meyerson, R.A. Weinberg, Nat. Med. 5 (1999) 1164–1170.
[5] J.W. Shay, W. Wright, Nat. Rev. Drug Discov. 5 (2006) 577–584.
[6] H. El-Daly, M. Kull, S. Zimmermann, M. Pantic, C.F. Waller, U.M. Martens, Blood 105 (2005) 1742–1749.
[7] J.W. Shay, W.N. Keith, Br. J. Cancer 98 (2008) 677–683.
[8] D. Sun, B. Thompson, B.E. Cathers, M. Salazar, S.M. Kerwin, J.O. Trent, T.C. Jenkins, S. Neidle, L.H. Hurley, J. Med. Chem. 40 (1997) 2113–2116.
[9] D. Monchaud, M.P. Teulade-Fichou, Org. Biomol. Chem. 6 (2008) 627–636.
[10] S.M. Gowan, J.R. Harrison, L. Patterson, M. Valenti, M.A. Read, S. Neidle, L.R. Kelland, Mol. Pharmacol. 61 (2002) 1154–1156.
[11] A.M. Burger, F. Dai, C.M. Schultes, A.P. Reszka, M.J. Moore, J.A. Double, S. Neidle, Cancer Res. 65 (2005) 1489–1496.
[12] M. Gunaratnam, O. Greciano, C. Martins, A.P. Reszka, C.M. Schultes, H. Morjani, J.F. Riou, S. Neidle, Biochem. Pharmacol. 74 (2007) 679–689.
[13] C. Leonetti, S. Amodei, C. D'Angelo, A. Rizzo, B. Benassi, A. Antonelli, R. Elli, M.F.G. Stevens, M. D'Incalci, G. Zupi, A. Biroccio, Mol. Pharmacol. 66 (2004) 1138–1146.
[14] D. Gomez, T. Wenner, B. Brassart, C. Douarre, M.F. O'Donohue, V. El Khoury, K. Shin-ya, H. Morjani, C. Trentesaux, J.F. Riou, J. Biol. Chem. 281 (2006) 38721–38729.
[15] P. Phatak, J.C. Cookson, F. Dai, V. Smith, R.B. Gartenhaus, M.F. Stevens, A.M. Burger, Br. J. Cancer 96 (2007) 1223–1233.
[16] Y. Mo, Y. Gan, Cancer Res. 63 (2003) 579–585.

[17] A. De Cian, L. Lacroix, C. Douarre, N. Temime-Smaali, C. Trentesaux, J.F. Riou, J.L. Mergny, Biochimie 90 (2008) 131–155.
[18] L. Oganesian, T.M. Bryan, BioEssays 29 (2007) 155–165.
[19] L. Janovec, M. Kozurková, D. Sabolová, J. Ungvarský, H. Paulíková, J. Plšíková, Z. Vantová, J. Imrich, Bioorg. Med. Chem. 19 (2011) 1790–1801.
[20] L. Janovec, D. Sabolová, M. Kožurková, H. Paulíková, P. Kristian, J. Ungvarský, E. Moravcikova, M. Bajdichova, D. Podhradsky, J. Imrich, Bioconjugate Chem. 18 (2007) 93–100.
[21] J. Plsikova, L. Janovec, J. Koval, J. Ungvarsky, J. Mikes, R. Jendzelovsky, P. Fedorocko, J. Imrich, P. Kristian, J. Kasparkova, V. Brabec, M. Kozurkova, Eur. J. Med. Chem. 57 (2012) 283–295.
[22] Z. Vantova, H. Paulíkova, D. Sabolova, M. Kozurkova, M. Suchanova, L. Janovec, P. Kristian, J. Imrich, Int. J. Biol. Macromol. 45 (2009) 174–180.
[23] M. Kozurková, D. Sabolová, L. Janovec, J. Mikeš, J. Koval', J. Ungvarský, M. Stefanisinova, P. Fedorocko, P. Kristian, J. Imrich, Bioorg. Med. Chem. 16 (2008) 3976–3984.
[24] R.J. Harrison, J. Cuesta, G. Chessari, M.A. Read, S.K. Basra, A.P. Reszka, J. Morrell, S.M. Gowan, C.M. Incles, F.A. Tanious, W.D. Wilson, L.R. Kelland, S. Neidle, J. Med. Chem. 46 (2003) 4463–4476.
[25] A.R. Allouche, J. Comput. Chem. 32 (2011) 174–182. Chemaxon: <http://www.chemaxon.com>.
[26] J.C. Phillips, R. Braun, W. Wang, J. Gumbart, E. Tajkhorshid, E. Villa, C. Chipot, R.D. Skeel, L. Kale, K. Schulten, J. Comput. Chem. 26 (2005) 1781–1802.
[27] W.L. Jorgensen, J. Chandrasekhar, J. Madura, M.L. Klein, J. Chem. Phys. 79 (1983) 926–935.
[28] J. Wang, P. Cieplak, P.A. Kollman, J. Comput. Chem. 21 (2000) 1049–1074.
[29] J. Wang, W. Wang, P.A. Kollman, D.A. Case, J. Mol. Graphics Modell. 25 (2006) 247.
[30] J. Wang, R.M. Wolf, J.W. Caldwell, P.A. Kollman, D.A. Case, J. Comput. Chem. 25 (2004) 1157–1174.
[31] R. Huey, G.M. Morris, A.J. Olson, D.S. Goodsell, J. Comput. Chem. 28 (2007) 1145–1152.
[32] G.M. Morris, D.S. Goodsell, R.S. Halliday, R. Huey, W.E. Hart, R.K. Belew, A.J. Olson, J. Comput. Chem. 19 (1998) 1639–1662.
[33] M.F. Sanner, J. Comput. Chem. 17 (1999) 57–61.
[34] N.H. Campbell, G.N. Parkinson, A.P. Reszka, S. Neidle, J. Am. Chem. Soc. 130 (2008) 6722–6724.
[35] E.F. Pettersen, T.D. Goddard, C.C. Huang, G.S. Couch, D.M. Greenblatt, E.C. Meng, T.E. Ferrin, J. Comput. Chem. 25 (2004) 1605–1612.
[36] W.F. Humphrey, A. Dalke, K. Schulten, J. Comput. Chem. 14 (1996) 33–38.
[37] A. Artese, G. Costa, S. Distinto, F. Moraca, F. Ortuso, L. Parrotta, S. Alcaro, Eur. J. Med. Chem. 68 (2013) 139–149.
[38] R. Ferreira, R. Artali, A. Benoit, R. Gargallo, R. Eritja, D.M. Ferguson, Y.Y. Sham, S. Mazzini, PLoS One 8 (2013) e57701.
[39] S. Alcaro, G. Costa, S. Distinto, F. Moraca, F. Ortuso, L. Parrotta, A. Artese, Curr. Pharm. Des. 18 (2012) 1873–1879.
[40] S. Alcaro, A. Artese, J.N. Iley, S. Missailidis, F. Ortuso, L. Parrotta, R. Pasceri, F. Paduano, C. Sissi, F. Trapasso, M.G. Vigorita, Chem. Med. Chem. 5 (2010) 575–583.
[41] F.S. Di Leva, E. Novellino, A. Cavalli, M. Parrinello, V. Limongelli, Nucleic Acids Res. 42 (9) (2014) 5447–5455.
[42] P. Akhshi, N.J. Mosey, G. Wu, Angew. Chem. Int. Ed. 51 (2012) 2850–2854.
[43] F. Fogolari, H. Haridas, A. Corazza, P. Viglino, D. Corà, M. Caselle, G. Esposito, L.E. Xodo, BMC Struct. Biol. 9 (2009) 64.
[44] H.H. Lee, W. Wilson, D.M. Ferry, P. Zijl, S.M. Pullen, W.A. Denny, J. Med. Chem. 39 (1996) 2508–2517.
[45] C.B. Carlson, P.A. Beal, Bioorg. Med. Chem. Lett. 10 (2000) 1979–1982.
[46] J.G. Delcros, S. Tomasi, S. Carrington, B. Martin, J. Renault, I.S. Blagbrough, P. Uriac, J. Med. Chem. 45 (2002) 5098–5111.
[47] S.F. Baranovsky, P.A. Bolotin, M.P. Evstigneev, D.N. Chenyshev, J. Appl. Spectrosc. 76 (2009) 132–139.
[48] H. Ihmels, D. Otto, Top. Curr. Chem. 258 (2005) 161–204.
[49] M. Kozurková, D. Sabolová, H. Paulíková, L. Janovec, P. Kristian, M. Bajdichová, J. Buša, D. Podhradský, J. Imrich, Int. J. Biol. Macromol. 41 (2007) 415–422.
[50] Y.L. Li, X.J. Luo, Q.P. Qin, Y.C. Liu, Z.F. Chen, Ind. J. Chem. 52 (2013) 486–491.
[51] M. Pietrzak, Z. Wieczorek, A. Stachelska, Z. Darzynkiewicz, Biophys. Chem. 104 (2003) 305–313.
[52] J. Kypr, I. Kejnovska, D. Renciuk, M. Vorlickova, Nucleic Acids Res. 37 (2009) 1713–1725.
[53] M.A. Ismail, K.J. Sanders, G.C. Fennell, H.C. Latham, P. Wormell, A. Rodger, Biopolymers 46 (1998) 127–143.
[54] A. Rodger, R. Marrington, M.A. Geeves, M. Hicks, L. de Alwis, D.J. Halsall, T.R. Dafforn, Phys. Chem. Chem. Phys. 8 (2006) 3161–3171.
[55] T. Ihara, T. Ikegami, T. Fujii, Y. Kitamura, S. Sueda, M. Takagi, A. Jyo, J. Inorg. Biochem. 100 (2006) 1744–1754.
[56] P.J. Chou, W.C. Johnson, J. Am. Chem. Soc. 115 (1993) 1205–1214.
[57] B. Norden, F. Tjerneld, Biophys. Chem. 4 (1976) 191–198.
[58] M. Wirth, O. Buchardt, T. Koch, P.E. Nielsen, B. Norden, J. Am. Chem. Soc. 110 (1988) 932–939.
[59] A. Rodger, K.J. Sanders, M.J. Hannon, I. Meistermann, A. Parkinson, D.S. Vidler, I.S. Haworth, Chirality 12 (2000) 221–236.
[60] D. Suh, J.B. Chaires, Bioorg. Med. Chem. 3 (1995) 723–728.
[61] E. Grueso, R. Prado-Gotor, Chem. Phys. 373 (2010) 186–192.
[62] S. Paramasivan, I. Rujan, P.H. Bolton, Methods 43 (2007) 324–331.
[63] C.C. Hardin, E. Henderson, T. Watson, J.K. Prosser, Biochemistry 30 (1991) 4460–4472.
[64] M. Chauhan, K. Banerjee, F. Arjmand, Inorg. Chem. 46 (2007) 3072.